Topical Review

Superconducting magnetic levitation: principle, materials, physics and models

P Bernstein◉ and J Noudem◉

Normandy University, ENSICAEN, CRISMAT Lab, CNRS 14050 Caen, France

E-mail: pierre.bernstein@ensicaen.fr

CrossMark

Abstract

In contrast to the interaction between two magnets with opposite magnetization directions, the interaction between a permanent magnet and a superconductor can be stable and result in magnetic levitation. This property can be exploited for the development of high velocity rotating bearings with no mechanical contacts and for the development of levitated trains. In this review, we focus on this latter application. After a brief description of the other techniques developed for levitating trains and the resulting achievements, we describe the magnet–superconductor interaction and recall the achievements in this field. We then give insights into the properties of the employed magnets and arrangement of magnets and we detail the characteristics and the fabrication processes of the most frequently used superconductors. Focusing on physics, we detail the procedures generally used for measuring the vertical (levitation) and the lateral (guidance) forces in magnetic levitation and the results obtained from experiments. We detail and give a critical review of the various models proposed for reproducing the force measurements. In the conclusion we discuss the possible future developments of the technology.

Keywords: levitation force, maglev, superconducting magnetic levitation

(Some figures may appear in colour only in the online journal)

1. Introduction

Magnetic interactions have played a key role in the development of electronic and electro-technical devices for more than a century. They are at the root of mass data storage in hard disks. They can generate strong forces or torques with no mechanical contact. This property, used in frictionless permanent magnet motors and generators, has led to the development of magnetic bearings for turbo-molecular pumps [1, 2] and other devices requiring a high rotating velocity [3]. In the field of rail transportation, since repulsive as well as attractive interactions are possible between two magnetized devices, the possibility of replacing the mechanical contact between wheels and rails by magnetic interactions has been investigated for many years. This saves energy, suppresses the costs related to the maintenance of the wheels and the rails and replaces noisy trains with silent ones. At first glance, the ideal device would comprise permanent magnets with opposite magnetization directions. Unfortunately, as stated by the Earnshaw theorem, magnetic systems with opposite magnetization directions are mechanically unstable [4–6]. To circumvent this difficulty, magnetic rotating bearings include electromagnets and a rotating shaft carrying magnets. The current in the electromagnets is modulated as a function of the location of the shaft in order to reduce as much as possible its excursion [7]. In the field of transportation, the Transrapid uses a similar principle for train levitation [8]. In the 1980s the development of NdFeB magnets and the discovery of high temperature superconductors (HTS) has opened up new possibilities since HTS, like the other type II superconductors, can be mechanically stable in a wide range of positions and orientations when interacting with a permanent magnet. In comparison, if magnetic levitation is achieved with a type I superconductor, the superconductor has a single defined equilibrium position about which it can only orbit or oscillate [9]. As a result, auto-stabilized rotating bearings have been

demonstrated with HTS and NdFeB magnets [10–13] and investigations into levitating trains have been carried out [14–25].

We describe briefly in section 2 the various magnetic levitation systems developed for railways but we focus on the one based on superconductor–magnet interactions. In section 3 we detail the characteristics of the magnetic and superconducting materials employed and the results of the experimental works carried out in this field. In section 4 we give a critical view of the different models developed for reproducing the behavior of a HTS in the field of a permanent magnet. In the conclusions, we detail the obstacles to the development of transportation systems based on this technology and the possibilities of overcoming them.

2. Magnetic levitation in railways

Three technologies have been developed for trains in magnetic levitation: electromagnetic levitation (EML), electrodynamic levitation (EDL) and superconducting magnetic levitation (SML). A common feature of all the technologies is that the trains are propelled by some type of linear motor. A detailed description of the realizations in this field up to now is given in [26].

2.1. EML

EML is based on the attractive force between ferromagnetic rails and electromagnets located below the rails and mechanically connected to the moving vehicles [8]. The first EML train, called Transrapid, was designed in Germany and tested on a 31.8 km guideway built in 1987 in Emsland. However, the Transrapid has been in commercial operations in China only. In the Transrapid system a 10 mm clearance between the rails and the electromagnets is monitored by sensors modulating the current in the electromagnets. The guidance is by other electromagnets located on both sides of the train. The commercial speed can be as high as 430 km h^{-1}. The first line was built in Shanghai and has been operational since 2004. Two other lines were constructed in China and have been operational since 2016 and 2017, respectively [27]. The construction of a 1000 km long line between the cities of Guangzhou and Wuhan is to begin in 2020 with trains running at an initial speed of 600 km h^{-1} [28]. Also, a 6.1 km long EML line was constructed in Korea at the Incheon airport and has been operational since 2016 [29]. EML trains are fast, silent and reliable. They are very efficient for connecting two locations, for example a downtown station and an airport. Their main disadvantage is the difficulty of designing a fast switch point, useful in a maintenance shed or for the connection of lines in an urban network.

2.2. EDL

EDL is based on the induction of currents in conductors by moving magnetic sources. Two main technologies have been developed.

The Chuo Shinkansen in Japan [30] carries low temperature superconducting coils at the end of its bogies (bogies are the frameworks attached to the vehicles that carry the axles). When the train is in motion, the field due to the currents in the superconducting coils induces currents in copper coils shaped like an '8' and located in walls built on both sides of the track. Facing coils are connected. At low speed the interaction between the field of the superconducting coils and the induced currents generates a drag force. As the train velocity increases, the drag force is replaced by a vertical one that, above 150 km h^{-1}, leads to the levitation of the train. The interaction forces between the currents in the copper coils and the field generated by the superconducting coils also provide the guidance of the train. The Chuo Shinkansen has reached a velocity of 603 km h^{-1}. The line under construction between Tokyo and Nagoya should be operational in 2025. The Chuo Shinkansen will then be the fastest commercial train in the world. The possibility of replacing the low temperature coils by HTS is investigated. As with the Transrapid, it suffers from the difficulty of designing fast switch points. In addition, the presence of the wheels and bogies could cause high maintenance costs.

The Indutrack carries Halbach arrays below the vehicles. Halbach arrays are described in section 3.1. They comprise a special arrangement of magnets and possibly soft iron pieces providing a large magnetic field. When the train is in motion, the field generated by the Halbach arrays induces currents in shorted conductors located along the guideway. These conductors are either coils or Litz-wire cables or stacks of either copper or aluminum foils punched in order so that they behave as shorted conductors. As for the Chuo Shinkansen, the interaction between the moving field of the Halbach arrays and the current induced in the conductors of the track creates a drag force at low velocity and a levitation force at high velocity. Small-scale mockups have been demonstrated [31] and Indutrack-like technology is planned for the levitation of the Hyperloop [32]. The object of this last project is the development of trains in levitation running in tubes under vacuum in order to suppress the energy losses due to the friction on air. The expected train velocity is in the 1000 km h^{-1} range. As with the Chuo Shinkansen, Indutrack trains cannot levitate below a certain velocity and require wheels in order to enter or exit stations.

2.3. SML

SML takes advantage of the large coercivity and remanent field of NdFeB permanent magnets, as well as of the properties of the superconducting materials of the YBa$_2$Cu$_3$O$_{7-\delta}$ (YBCO) family. These HTS present (i) a high critical temperature T_c; (ii) a high critical current density J_c and (iii) a moderate sensitivity to an applied magnetic field. When a HTS (or more generally a type II superconductor) is cooled

Figure 1. The Maglev Cobra on its guideway at the Federal University of Rio de Janeiro. The cryostats are visible below the vehicle. The wheels have been installed to protect the vehicle during the tests (photography by the authors).

down in the field of a permanent magnet at some distance z_{cp} from the permanent magnet, in a process called field cooling (FC), vortices enter the superconductor at T_c. Since no shielding currents flow in the superconductor, no force is generated at z_{cp} whatever $T \leqslant T_c$. If the respective positions of the permanent magnet and the superconductor change, shielding currents are generated in order to restore the field existing in the superconductor at the cooling point. If z, the magnet–superconductor separation, increases (resp. decreases), an attractive (resp. repulsive) force occurs. If there is a lateral motion of either the magnet or the superconductor, a guidance force aiming at bringing the system back to the position it had when it was cooled down is generated. In summary, in SML, the forces between the permanent magnet and the superconductor make the system stable. It is often said that the stability is due to the vortices that are pinned in the superconductor. It is true that the levitation and the guidance forces are reduced if vortices are depinned. However, the levitation and guidance forces are due to the current distribution in the superconductor, which explains why they can be reproduced by models and simulations techniques determining this distribution (see section 4). The first demonstration of a SML vehicle was made at the Southwest Jiaotong University in Chengdu, China, in 2002 [14], which has been a leading center for the development of this technology ever since [15–17, 21–23, 25, 33–38]. Various small scale vehicles levitating above a short magnetic guideway circuit were built and tested, especially in Chengdu and at IFW in Dresden, Germany. A real scale guideway and vehicle were built at the Federal University of Rio de Janeiro, Brazil [26, 39–41]. The guideway, that is 200 m long, was built according to a Halbach design. The vehicle, called Maglev Cobra, comprises four cars and is levitated by 24 cryostats including YBCO bulks [40, 42, 43] (see figure 1). It can carry 30 passengers and has been in operation for demonstrations once a week since 2014. The cryostats were built by the ATZ company [44] and were designed to carry up to 2500 N [45, 46]. Each of them contain 24 three-seeded YBCO bulks in two rows [47, 48] (see figure 2).

SML trains do not need wheels to enter and exit the stations and the respective position of the superconductors and the guideway make fast switch points conceivable. The superconductors are cooled down to 77 K with liquid nitrogen and can be kept at this temperature for 40 h in static conditions according to the manufacturer [44]. In operational conditions, however, the time interval between two nitrogen fillings is somewhat reduced.

These trains are well suited to urban transportation networks requiring repeated acceleration and deceleration phases. Disadvantages are that they require magnets for the guideway and superconductors for levitating the vehicles, which are both expensive.

3. SML: experimental aspects

The characterization of levitation has been achieved on single superconducting bulks as well as on cryostats containing an assembly of superconductors. It requires the measurement of the vertical levitation force as a function of the separation between the magnetic source and the superconductor, as well as that of the levitation and guidance forces as functions of lateral displacements. These last measurements are essential for the design of a SML transportation system. Moving vehicles are subject to a centrifugal force in the curved sections of the guideway and the guidance force must be large enough to keep the vehicle on track in any case. Typically, in the railway industry, the centrifugal acceleration must be kept below $1\ \mathrm{m\,s^{-2}}$ for the comfort of the passengers. This means that the ratio of the guidance to the levitation forces must at least be equal to 10%, plus a safety margin. Otherwise, the lateral position of the train above the guideway can change due to the repeated motion of the train above the curved sections and there is a natural decay of the levitating height over time due to the thermal depinning of the vortices. In order to restore the normal levitation height and position of the trains, the superconductors in the cryostats must be heated up to a temperature higher than T_c and cooled down to 77 K at z_{cp}. How far the decay of the levitating height and the gap between the normal and actual locations of the train are enlarged by vibrations and other perturbations must be estimated for the safety of the planned SML system and in order to determine the time interval between two heating and field cooling cycles. In addition to their obvious practical interest, the results of these measurements provide insights into the physics of magnetic levitation and provide a bench test for the relevance of the proposed models.

In this section, we examine the effects of various factors on the levitation and guidance forces. We describe firstly the magnetic sources and the superconducting materials used in SML systems and investigations on magnetic levitation, then we address the measurements procedures before detailing the results obtained.

3.1. The magnetic field sources

3.1.1. $Nd_2Fe_{14}B$ magnets [49–51]. $Nd_2Fe_{14}B$ (NdFeB) permanent magnets were discovered in 1983. NdFeB is a tetragonal compound with lattice constants a $= 0.88$ nm and

(a)   (b)
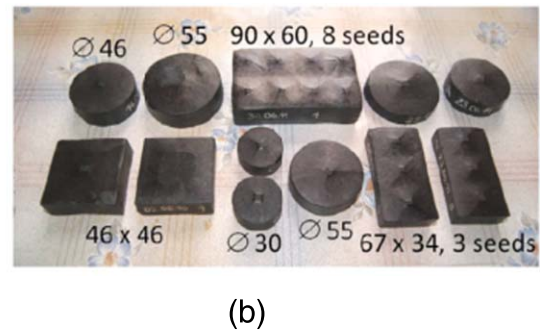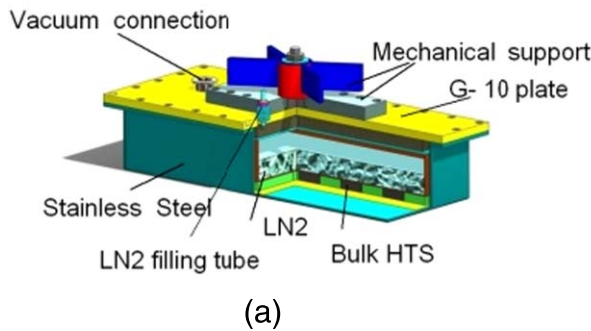
Figure 2. (a) Schema of the ATZ cryostat levitating the Maglev Cobra [43]. (b) Top seeded bulks fabricated by the ATZ company. The three-seeded YBCO bulks are visible on the right in the lower part of the figure. Reproduced from [48]. © IOP Publishing Ltd. All rights reserved.

c = 1.221 nm, the space group of which is $P4_2/mnm$. The unit cell contains 68 atoms. Almost all the Fe atoms are located in Fe layers while Nd and B atoms are located in other layers separated from each other by Fe layers. The magnetic moment per formula unit is equal to 32.5 μ_B at 300 K and the Curie temperature to 586 K. Usually, the compound includes other rare-earth atoms, especially Dy, to improve coercivity. NdFeB crystallites show a high magnetic uniaxial anisotropy. According to the fabrication technique, there are two types of NdFeB magnets: the sintered magnets that show the best magnetic properties and the bonded magnets. The Halbach arrays are generally built with bonded magnets that are more easily given the shape required for the application, and are cheaper. The main advantages of NdFeB bonded magnets for SML are their large coercivity and remanent magnetization that can be as high as 1200 kA m^{-1} and 0.7 T, respectively.

3.1.2. Halbach arrays [52].
The Halbach arrays consist of an arrangement of magnets or of magnets and soft iron pieces that concentrates the magnetic flux. Often they are designed in order that the flux is larger along one face of the arrangement than along the opposite face. If iron pieces are present, the flux of several magnets is concentrated in the iron pieces, increasing the field above these pieces to well above the field that a single permanent magnet could generate. Examples of Halbach arrays can be seen in figures 16 and 17.

3.2. The superconducting materials

Several families of superconductors could be *a priori* interesting for magnetic levitation, especially the compounds containing Bi, those of the YBCO family and MgB$_2$. However, early on after the discovery of the HTS, measurements of the levitation force of (Bi,Pb)$_2$Sr$_2$Ca$_2$Cu$_3$O$_x$ samples have shown that this material was not as promising as YBCO for the application [53]. In this section, we detail the properties and the fabrication processes of (i) bulks of the YBCO family and (ii) the MgB$_2$ ceramic. These materials are the most commonly used superconductors in the investigation of magnetic levitation and for the development of levitation systems.

3.2.1. YBCO and (RE)BCO bulks: structural properties.
YBa$_2$Cu$_3$O$_{7-\delta}$ $(0 \leqslant \delta \leqslant 1)$ compounds have a distorted
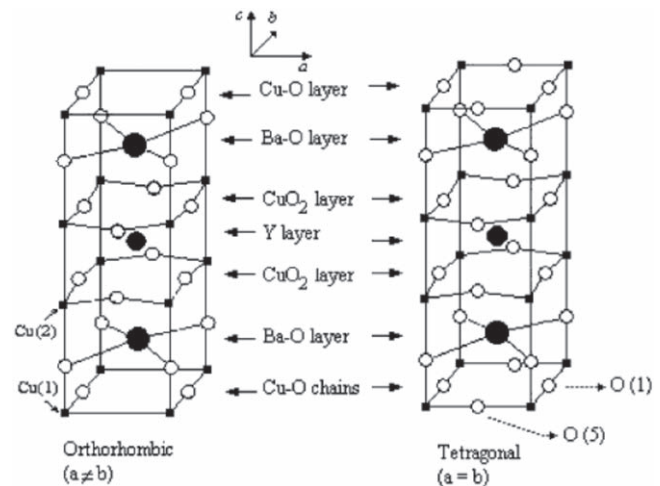

Figure 3. Crystal structures of the orthorhombic and tetragonal phases of YBCO. Reprinted from [56], Copyright (2004), with permission from Elsevier.

oxygen-deficient perovskite structure. For $\delta \geqslant 0.6$ YBCO is tetragonal (see figure 3) and non-superconducting, but a transition to a superconducting orthorhombic structure occurs for $\delta < 0.6$. The lattice parameters of the orthorhombic structure are: a = 0.3283 nm, b = 0.3886 nm and c = 1.168 nm and the space group is Pmmm [54, 55]. The unit cell is a triple perovskite structure with ordered oxygen vacancies at the central yttrium site and the basal copper site. The Y and Ba atoms are occupying crystallographic sites with eight fold and ten fold coordination to O atoms, respectively. The resistivity ρ of the tetragonal phase shows a semiconducting behavior as a function of the temperature. The orthorhombic phase is superconducting and $\rho(T)$ shows a metallic resistivity trend (see figure 4), because the carriers density in the Cu–O planes increases with the oxygen content [57]. Accordingly, T_c depends on δ (see figure 5) i.e. it depends on the carrier concentration [58]. Since the superconducting electrons are located in the Cu–O planes, the superconducting properties are anisotropic. The bulks produced by sintering or by melt growth are tetragonal. They must be slowly cooled or post-annealed around 500 °C for 72 to 100 h in an oxygen atmosphere in order to be superconducting. Rare earths (RE), with the exception of Ce and Pm, can be substituted to yttrium without destructive
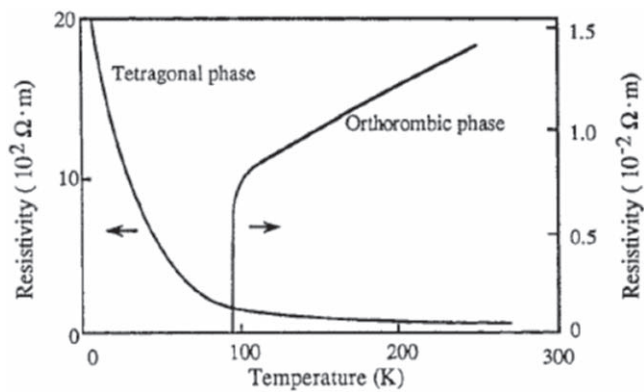
Figure 4. Temperature dependence of the resistivity for the orthorhombic and tetragonal phases in Y123. Reproduced from [57]. © IOP Publishing Ltd. All rights reserved.
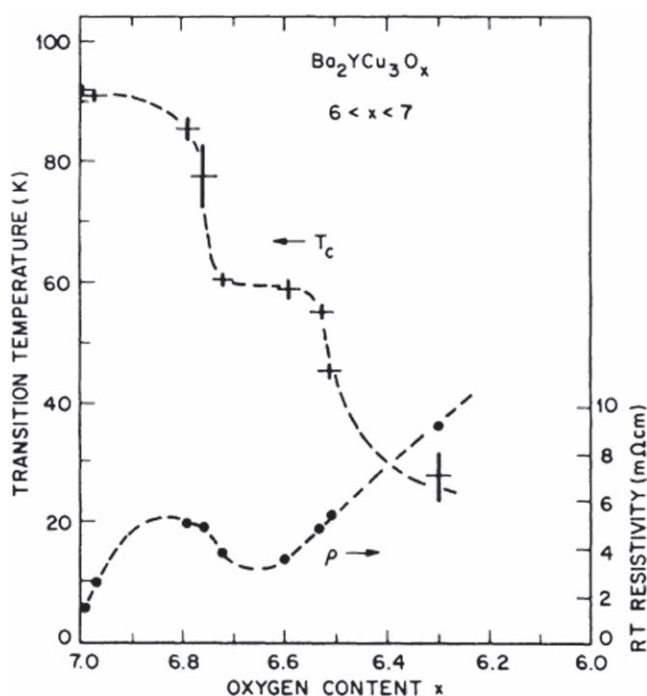

Figure 5. Dependence of T_c on oxygen content in Y123. Also shown is the resistivity at 300 K. Reprinted figure with permission from [58], Copyright (1987) by the American Physical Society.

effects on the superconducting properties [59–63]. There are relations linking the ionic radius of the RE ion to T_c, the lattice parameters of the substituted phase and the peritectic temperature, T_p [62–65]. In general, T_c and T_p increase with increasing ionic radius. However, above a certain threshold, further increase in the ionic radius induces a T_c decrease because RE ions substitute easily into the Ba sites [66–68]. (RE)BCO phases including RE elements with a large magnetic moment can be superconducting, which is in conflict with the Bardeen–Cooper–Schrieffer theory.

3.2.2. YBCO and (RE)BCO bulks: fabrication processes. Although sintering is very common and has many advantages in ceramic processing, it has failed to produce oxide superconductors with a high critical current density, mainly

because of the presence of weak links at the grain boundaries. Melt solidification processes have overcome this problem by texturing the material and improving (i) the grain orientation, (ii) the grain boundaries conductivity and (iii) flux pinning. As a result, the obtained J_c was strongly increased. The chemical formation of YBCO is a peritectic reaction in which solid Y_2BaCuO_5 (Y211) reacts with the liquid $BaCuO_2 + CuO$ phase (L phase). The peritectic temperature T_p is equal to 1002 °C. The phase diagram shows that another peritectic reaction exists in this pseudo-binary system. If cooled down from a temperature above 1230 °C, Y_2O_3 reacts peritectically at or below 1230 °C with the L phase, resulting in the formation of solid Y211, which acts as a properitectic phase for the peritectic $YBa_2Cu_3O_y$. In the following, we give insights into the various melt processing techniques developed for the fabrication of YBCO and (RE)BCO bulks. These techniques have led to the fabrication of (i) disks with a maximum diameter in the 150 mm range [69] and (ii) up to 100 mm long bars with a 10 mm diameter [70].

3.2.2.1. Melt textured growth (MTG). MTG was initiated by Jin *et al* [71]. A sintered YBCO sample was melted above T_p at 1050–1200 °C to decompose into the Y211 and L phases. After melting, the mixture was cooled down in a 20–50 °C cm^{-1} thermal gradient. The resulting YBCO grains were shaped as needles 100 to 300 mm long. The critical current density exceeded 10 kA cm^{-2} at 77 K in self field. This was the signature that grain alignment had probably eliminated the weak links. However J_c was small when a magnetic field was applied, suggesting that flux pinning was insufficient. In order to improve flux pinning with Y211 particles, various versions of melt processing were developed.

3.2.2.2. Liquid phase processing. This method was reported by Salama *et al* [72]. A sintered YBCO bar is introduced vertically into a furnace at 1100 °C in order to heat up and decompose the bar rapidly. After 15 to 30 min holding time the bar is cooled down rapidly to a temperature slightly above T_p and subsequently cooled down to 925 °C at 0.5–2 °C h^{-1}. This process aims at limiting the coarsening of the Y211 particles and retaining a minimum particle size before solidification of the YBCO phase.

3.2.2.3. Quenched melt growth (QMG) and melt power melt growth (MPMG) [73, 74]. The QMG/MPMG processes have been developed to control the size of the Y211 particles and, taking the phase diagram into consideration, to make these particles more effective flux pinning centres.

In the QMG process a sintered YBCO sample is heated up to the $Y_2O_3 + L$ region of the phase diagram and splat quenched using cold copper blocks. The quenched plates are subsequently heated up to the Y211 + L region, where the Y211 phase is produced by a peritectic reaction between Y_2O_3 and the L phase. Since Y211 nucleates from Y_2O_3, it is possible to control the size distribution of the Y211 grains if that of the Y_2O_3 grains is controlled.

In the MPMG process, the melt quenched plates are crushed into a fine powder and well mixed. As a result, coarse Y_2O_3 grains are refined with a uniform distribution. The pellets are subsequently rapidly heated up to the Y211 +L region.

In both processes, after 20 min to 1 h holding time, the sample is rapidly cooled down to a temperature just above T_p and then cooled down to 850–950 °C at 0.5–5 °C h^{-1}. The microstructure of QMG and MPMG processed samples consists of small spherical 211 particles ($<2\,\mu$m) distributed in the YBCO matrix. The volume fraction of Y211 particles depends on the Y element content in the starting material.

3.2.2.4. Power melting process (PMP) and solid liquid melt growth (SLMG) process [75, 76]. Other techniques based on slow cooling from a temperature above T_p have been developed. Instead of using melt quenched powder, as in QMG and MPMG, two processes termed PMP and SLMG have been proposed.

The PMP process consists of using a mixture of Y_2O_3/CuO and $BaCuO_2$ for texturing. The resulting microstructure of PMP is similar to that of QMG processed samples. In the SLMG process, Y211, CuO and $BaCuO_2$ are used as precursors. The obtained microstructure is similar to that of MTG samples

3.2.2.5. Texturing by solidification in a magnetic field [77]. This process is based on the magnetic susceptibility anisotropy of YBCO and (RE)BCO. During solidification, the particles rotate in order to align their c-axis parallel to the applied magnetic field.

3.2.2.6. Top-seed melt texture growth (TSMTG) process. The TSMTG method consists of melting the material and then recrystallizing it by slow solidification, controlling the nucleation sites and the growth orientation with a high melting point seed located on top of the bulk preform before processing [78]. The seed is a (RE)BCO phase with a higher peritectic temperature than that of the desired YBCO or (RE)BCO phase [79, 80]. The TSMTG technique has enabled one to obtain monodomains YBCO or (RE)BCO samples with a maximum diameter in the 150 mm range [69] and presenting high performances [81, 82]. This method is used by various companies to grow commercial YBCO and (RE)BCO bulks [44, 83]. Bulks fabricated by TSMTG can be seen in figure 2(b).

As final observations on the fabrication of YBCO and (RE)BCO bulks, the fabrication processes are time demanding and the fabrication of large samples with uniform good superconducting properties is difficult.

3.2.3. MgB$_2$. This compound has been known since 1953 [84]. The superconductivity of MgB_2 below 39 K was reported in 2001 by Nagamatsu *et al* [85]. The main advantages of MgB_2 are its low cost, its low density (2.6 g.cm^{-3}) and its good mechanical properties [86, 87]. The critical current density is in the 2.10^5 A cm^{-2} range in
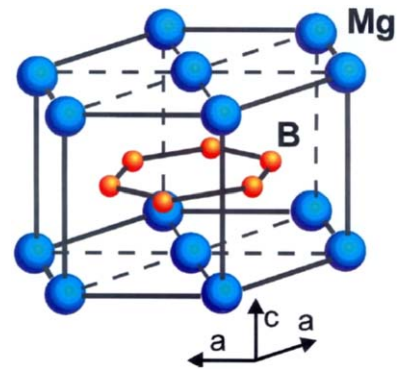

Figure 6. Crystal structure of MgB2.

self field at 25 K, a well suited temperature for applications employing MgB_2 bulks and exceeds 4.10^5 A cm^{-2} below 10 K [88, 89]. For comparison, the critical current density of YBCO in self field at 77 K is in the 10^4–10^5 A cm^{-2} range [90, 91] and approaches 10^6 A cm^{-2} below 20 K [92, 93]. The main disadvantage of MgB_2 is the fast decrease of J_c in the presence of an increasing applied field [88, 89] while even at 77 K the decrease of J_c in YBCO and (RE)BCO bulks is much lower [90, 93].

The crystal structure of MgB_2 is shown in figure 6 [85]. It is a simple binary compound that has a hexagonal AlB_2 type structure (space group P6/mmm) with unit cell parameters $a = 0.308$ nm and $c = 0.352$ nm [94]. The unit cell consists of alternating hexagonal layers of magnesium atoms and graphite-like honeycomb layers of boron atoms. The boron planes are separated by the layers of magnesium, and the magnesium atoms are closely packed with each magnesium atom located between the centres of the hexagons forming the boron lattice planes. In the boron layers, each hexagon consists of six boron atoms, giving an overall 1:2 Mg-B ratio in the unit cell. The structure of MgB_2 is anisotropic and the in-plane B-B distance is significantly shorter than the distance between two layers.

Basically, the preparation techniques of the other superconductor bulks can be applied to MgB_2. One of the main advantages of MgB_2 is that its formation occurs at relatively low temperatures with a high grain connectivity. As a result, good isotropic superconducting properties, especially a high J_c, can be obtained [95]. Spark plasma sintering (SPS) [96–99] is the most effective technique for fabricating MgB_2 bulks. This technique combines high current pulses (up to 10 kA) and mechanical pressure (up to 200 MPa) to consolidate under vacuum the MgB_2 powder located in a die (usually in conducting graphite). The current flows mostly in the die if the powder is insulating and in the powder itself if it is conducting. If the powder is insulating, it is heated up by the Joule effect. If it is conducting enough it has been suggested that, in addition to Joule heating, a plasma generated by sparks between grains facilitates the chemical reactions between the components of the powder and contribute to the soldering and the compaction of the grains [100]. There is no consensus on this issue. The whole process can last no longer than 30 min. MgB_2 bulks with various
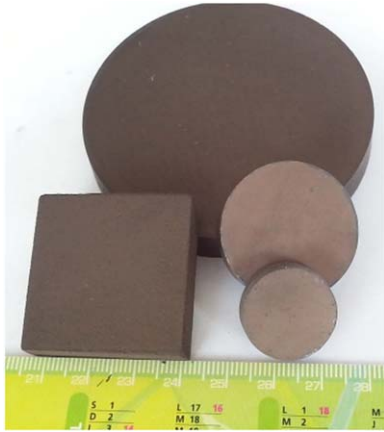
Figure 7. MgB$_2$ bulks fabricated at CRISMAT Lab with the SPS technique.

shapes and dimensions can be manufactured [101] (see figure 7). The obtained samples usually show a density larger than 98% and a very high hardness. In principle, the maximum size of the manufactured MgB$_2$ bulks depends on that of the SPS machine only.

3.3. The measurement procedures

To optimize the guidance and levitation forces and ensure that the safety conditions of the planned SML systems are fulfilled in any conditions, it is necessary to fully characterize these forces. The levitation force can be measured either in field cooling (FC) or in zero field cooling (ZFC) conditions. As mentioned in section 2.3, the levitation of SML trains is achieved in FC conditions. We consider firstly the simplest setup consisting of a superconductor in the normal state and a permanent magnet. In FC, while the distance z between the magnet and the superconductor is kept equal to z_{cp}, the superconductor is cooled down to the measurement temperature $T < T_c$ (step 1 in figure 8). After temperature stabilization, according to the measurement setup, either the magnetic source or the superconductor is moved vertically in order to reduce z down to z_{min} (step 2 in figure 8). At z_{min} the direction of motion is reversed and distance z increases up to z_{max} (step 3 in figure 8). The force of interaction between the permanent magnet and the superconductor is recorded as a function of z during the whole process. In ZFC, after cooling down the superconductor in a field as near to zero as possible, the procedure is the same as in FC. Some authors call field cooling measurements the determination of the attractive force while the distance between the magnetic source and the superconductor is increased after the field cooling step. This is not the definition we use here.

For measuring the guidance force, after the field cooling step, the superconductor is located at distance z from the magnetic source. Starting from $y = 0$, either the magnetic source or the superconductor is moved laterally at distance y from the initial position up to y_{max} where the direction of motion is reversed and distance y decreases down to y_{min} before increasing to zero (see figure 9).

The development of SML vehicles has required the measurement of the levitation and guidance forces of cryostats containing several superconductors and located above various magnetic sources, especially Halbach guideways. Special setups able to measure levitation and guidance forces in the several thousand newtons range were constructed for this purpose [33, 39, 102]. Figure 10 shows a drawing and a picture of the setup constructed at the Federal University of Rio de Janeiro. The measurement procedures with these systems are identical to those described above.

3.4. Knowledge gained from the measurements

In this section, we examine the effects of various factors on the levitation and guidance forces.

3.4.1. Effects of the cooling height on the levitation and guidance forces. Wang *et al* have shown that the levitation force of YBCO bulks above an Halbach arrangement of magnets is an increasing function of the cooling height [34] while measurements of the guidance force of a three seeded YBCO bulk by Dias *et al* [103] in similar conditions have shown that the guidance force is a decreasing function of z_{cp}. These are general results verified for systems using either magnets or other sources of magnetic field and bulk superconductors [104].

3.4.2. Effects of the dimensions of the permanent magnet and of the superconductor on the levitation force. Considering cylindrical permanent magnets and bulk superconductors for the sake of simplicity we examine firstly the effects of the size of the permanent magnet on the levitation force, then we discuss those of the size of the superconductor.

3.4.2.1. Effects of the diameter of the permanent magnet. Yang *et al* [105] have measured the levitation force between a YBCO bulk superconductor with a diameter $d_s = 18$ mm and permanent magnets with diameters d_{pm} ranging between 10 and 30 mm. They have shown that the interaction force first increases as the ratio $\frac{d_{pm}}{d_s}$ increases, is maximum for $d_s = d_{pm}$, then decreases for $d_{pm} > d_s$. The increase in the levitation force for increasing d_{pm} while $d_s > d_{pm}$ is attributed to the increased fraction of the superconductor surface magnetized by the magnetic field. The subsequent reduction for $d_s < d_{pm}$ is ascribed to the reduction of the magnetic field gradient as the diameter of the permanent magnet increases.

3.4.2.2. Effects of the permanent magnet thickness. The effect of the magnets' thicknesses was investigated in our lab [106] with 50 mm diameter magnets and a 70 mm diameter MgB$_2$ bulk. The measurements were carried out at 25 K after field cooling the superconductor at 45 mm from the magnets. They have shown that the levitation force first increases as the thickness h_{pm} of the permanent magnet increases, then tends towards saturation values (see figure 11(a)), as does the field along the axis of the magnets (figure 11(b)). Similar results were obtained with 60 mm diameters magnets. If the
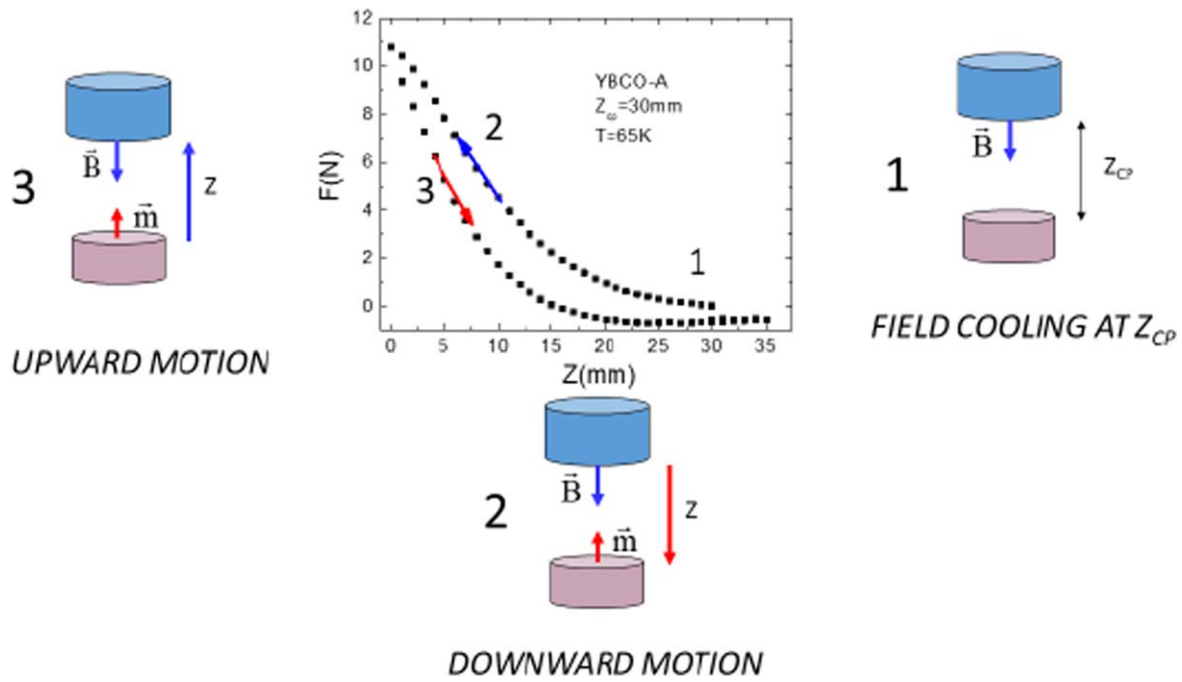
Figure 8. Measurement of the levitation force: after FC at z_{cp}, the superconductor is moved vertically down to z_{min}. At z_{min} the direction of motion is reversed and distance z increases up to z_{max}. The graph is the force hysteresis loop at 65 K of a 17.4 mm diameter YBCO disk cooled down at $z_{cp} = 30$ mm.
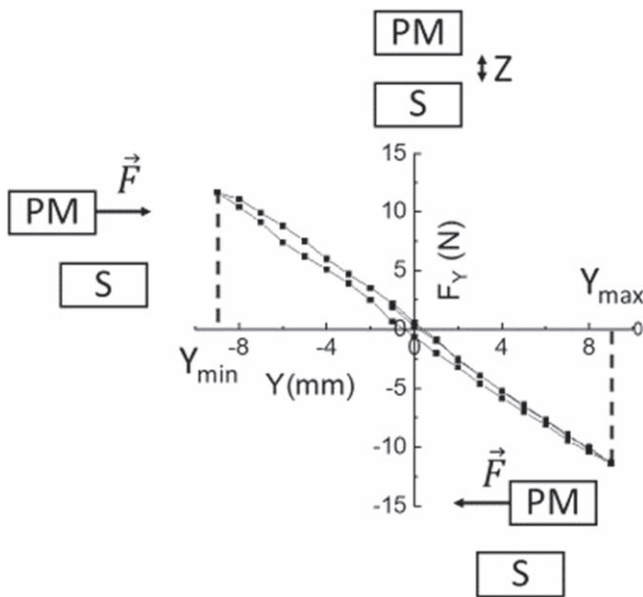

Figure 9. Measurement of the guidance force: after FC at z_{cp}, the superconductor is located at distance z from the magnetic source. Starting from $y = 0$, either the magnetic source or the super-conductor is moved laterally to y_{max} where the direction of motion is reversed and distance y decreases down to y_{min} before increasing to zero. The figure shows the respective positions of the magnetic source (PM) and of the superconductor (S) as well as the guidance force $\vec{F}$ at different steps of the measurement procedure. The graph is an example of the obtained curves.

permanent magnet diameter d_{pm} is equal to or larger than that of the superconductor, the levitation force is strongly connected to the field along the permanent magnet axis. This is illustrated in figure 12(a) that shows the levitation

force at 25 K between the 70 mm diameter superconductor and (i) a 100 mm diameter permanent magnet 20 mm thick and (ii) a 70 mm diameter permanent magnet with a thickness of 35 mm. Figure 12(b) shows the field created along their axis by the two magnets. The field and the field gradient of the 100 mm diameter permanent magnet are much less than those of the 70 mm one, as are the corresponding levitation forces. This results from the effect of the demagnetizing factor that is larger for a magnet with a large $\frac{d_{PM}}{h_{PM}}$ ratio than for a magnet with a smaller one.

3.4.2.3. Effects of the diameter of the superconductor. Considering situations in which $d_s \leqslant d_{pm}$, it is sometimes assumed that the levitation force is proportional to the superconductor surface. We have measured in our lab [106] the levitation force between a 70 mm diameter permanent magnet and 10 mm thick MgB$_2$ bulks with various diameters d_s. The superconductors were cooled down at $z_{cp} = 35$ mm from the magnets.

Figure 13(a) shows the force measured at 25 K when the magnet–superconductor separation was equal to 10 mm as a function of the bulk diameter. Clearly, the levitation force increases with d_s^3, not with d_s^2 while, as mentioned above, Yang *et al* have shown that for a given superconductor the levitation force decreases for $d_s > d_{pm}$ [105]. This behaviour is quite different from that of the trapped field. Figure 13(b) shows the field trapped along the bulks axis at a distance of 10 mm after cooling them down to 25 K with the same magnet–superconductor separation. As is consistent with the Bean model [107], the trapped field increases as a linear function of the superconductor diameter as far as $d_s < d_{pm}$.
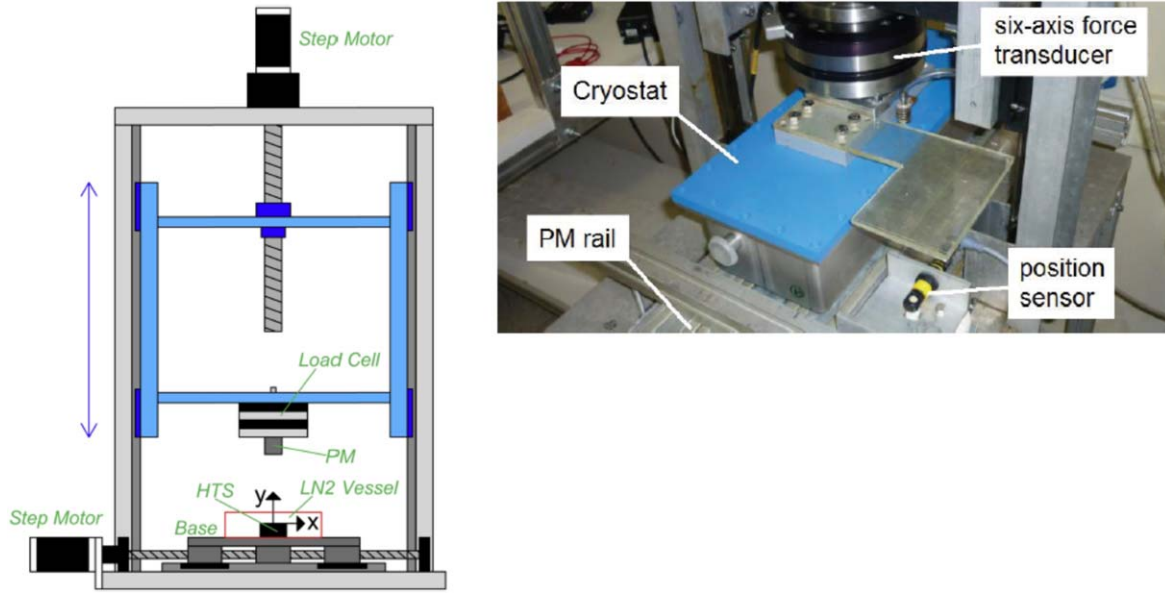
Figure 10. Drawing and photo of the set up constructed at the Federal University of Rio de Janeiro for the measurement of the guidance and levitation forces of cryostats containing several superconductors. Left image reprinted from [39], Copyright (2012), with permission from Elsevier. Right image reproduced from [102]. © IOP Publishing Ltd. All rights reserved
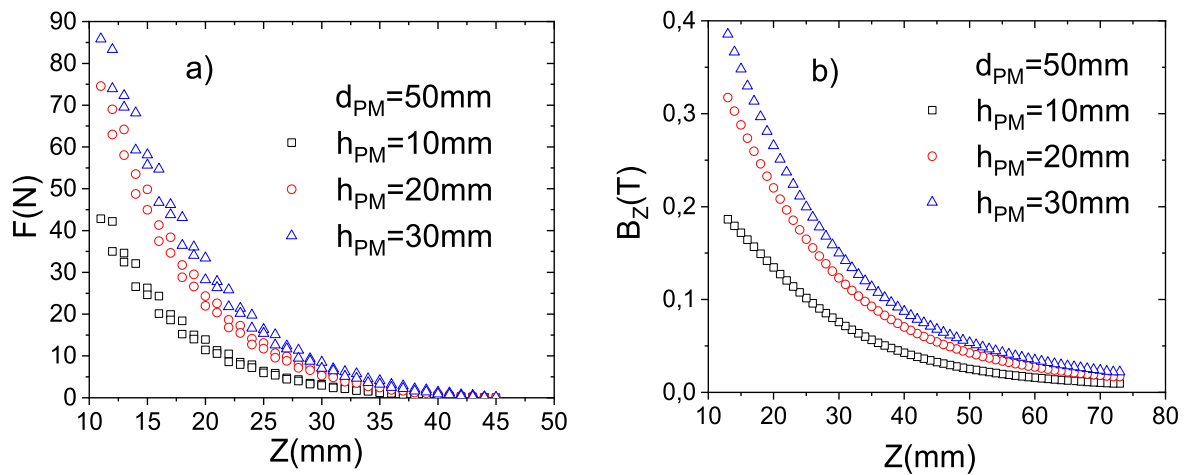

Figure 11. (a): Levitation force between a 70 mm diameter MgB_2 bulk and 50 mm diameter NdFeB magnets with various thicknesses, h_{pm}. The measurements were carried out after cooling the superconductor down to 25 K at 45 mm from the permanent magnet [106]. (b) Field generated by the magnets of figure 11(a) along their axis [106].

3.4.3. Effects of the temperature on the levitation force and the shape of the hysteresis loops. The temperature has strong effects on the levitation force and the hysteresis loops of the superconductors. In ZFC conditions Zhou *et al* have shown that the levitation force of YBCO bulks increases firstly as the temperature decreases, then tends towards saturation [108]. Bernstein *et al* [109] have obtained similar results on FC YBCO and MgB_2 bulks (see figure 14). The saturation is attributed to the levitation force approaching the Meissner limit for large J_c, i.e. a situation in which the currents flow on the surface of the superconductor only [110, 111]. Otherwise, the hysteresis loops of the levitation force are large near T_c and decrease as the temperature decreases [108, 109] (see figure 15). We emphasize that near T_c, the levitation force can decrease if the permanent magnet comes close to the superconductor.

3.4.4. Effects resulting from the design of the Halbach array.
A Halbach array is supposed to provide a larger levitation force than a classical arrangement of magnets. Measurements by Jing *et al* [35] support this point of view. They have compared the levitation force between two types of guideways and an arrangement of seven 30 mm diameter YBCO bulks with a thickness of 18 mm field cooled at 30 mm from the guideways. The schemas of the guideways can be seen in the left part of figure 16 and the arrangement of superconductors in the right part.

The right part of figure 16 also shows the obtained forces that are much larger with the Halbach array than with the
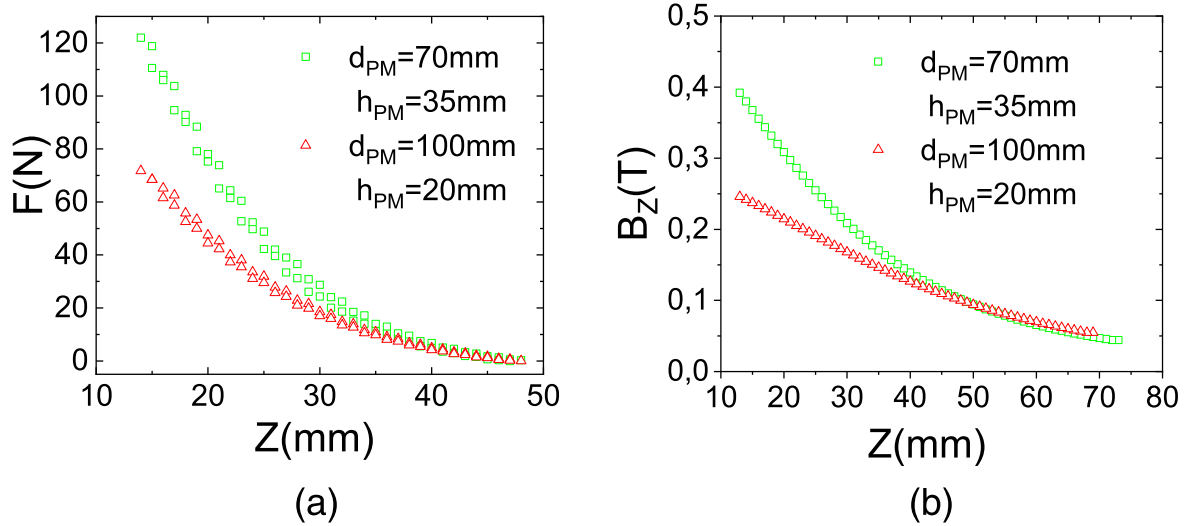
Figure 12. (a) Levitation force between a 70 mm diameter superconductor and (i) a NdFeB 100 mm diameter permanent magnet 20 mm thick and (ii) a 70 mm diameter NdFeB permanent magnet with a thickness of 35 mm [106]. (b) Field generated by the magnets of figure 12(a) along their axis [106].
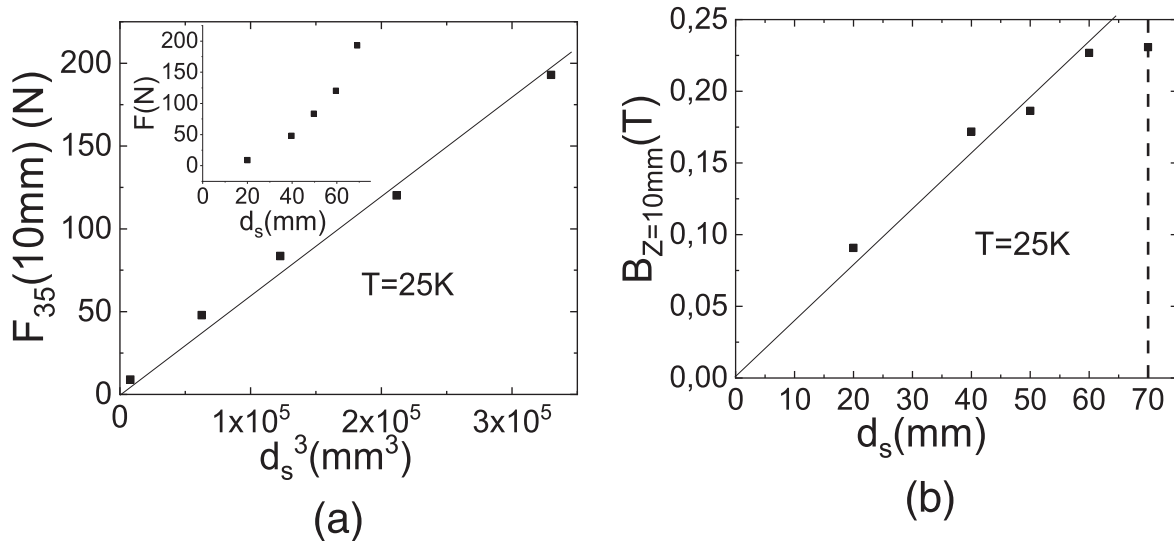

Figure 13. (a) Levitation force at 25 K between a 70 mm diameter permanent magnet located 10 mm away from bulk MgB$_2$ superconductors with diameter d_s as a function of $d_s{}^3$. The inset shows the levitation force as a function of d_s. The separation between the permanent magnet and the superconductors was equal to $z_{cp} = 35$ mm when the superconductor was cooled down [106]. (b) Field trapped by MgB$_2$ superconductors as a function of their diameter d_s. The superconductor was cooled down and the trapped field measured at a distance of 10 mm from the bulks [106].

other guideway. Del Valle *et al* [112], however, have shown that if a rectangular superconductor covers the entire surface of the guideway, a non-Halbach arrangement of magnets can result in a larger levitation force than a Halbach one, while this last one provides a better guidance force. The authors conclude that determining the most advantageous guideway can only be done taking into account the shape and the characteristics of the levitating superconductors. This work was carried out by Sotelo *et al* [40] for the ATZ cryostats of the Maglev-Cobra. They have compared the levitation and guidance forces provided by the five guideways shown in figure 17 and concluded that designs D and E provided the largest levitation force.

3.4.5. Effect of vibrations and vertical and lateral repetitive displacements on the levitating height and the levitation and guidance forces.. Since vortex depinning can be important at liquid nitrogen temperature in high temperature superconductors, the effects of magnetic relaxation on the levitation and guidance forces are not negligible. Magnetic relaxation occurs in static conditions, which means that the levitation force and the height of levitation of an isolated magnet-superconductor system decrease along time. For designing an operational SML system, the effects of vertical vibrations and repetitive vertical and lateral displacement must also be taken into account. Vibrations can be due to the inhomogeneity of the field generated by the guideway. Repetitive vertical displacements can result from passengers
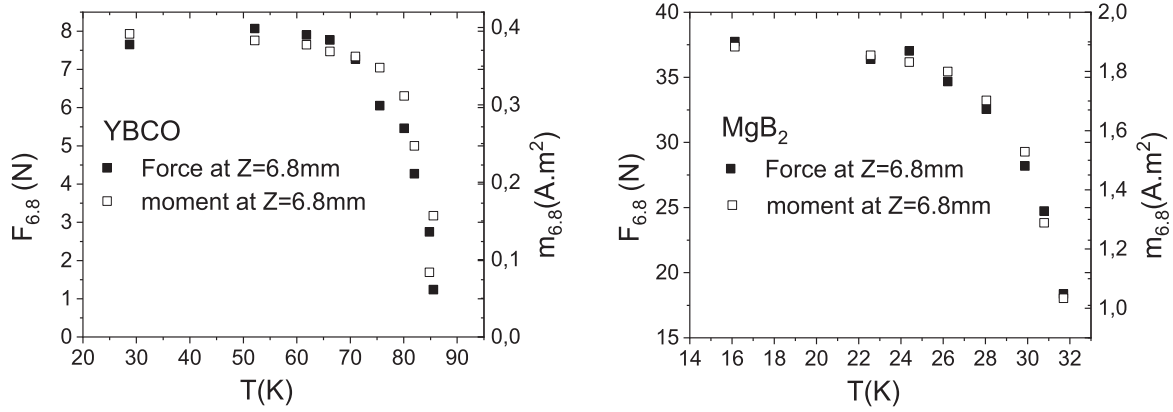
Figure 14. Levitation force and magnetic moment at 6.8 mm from a 35 mm diameter NdFeB permanent magnet as functions of the temperature of (i) a 17.4 mm diameter YBCO disk and (ii) a 35.6 mm diameter MgB$_2$ bulk cooled down at $z_{cp} = 35$ mm. Reproduced from [109]. © IOP Publishing Ltd. All rights reserved. The magnetic moment is calculated with equation (23) replacing B by ΔB_a (equation (24)).
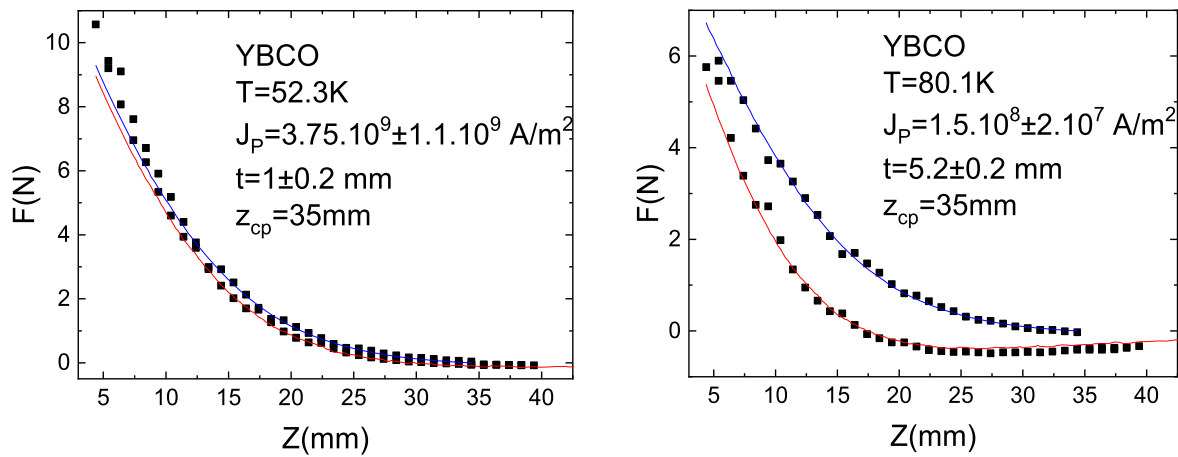

Figure 15. Force hysteresis loops of a 17.4 mm diameter YBCO bulk cooled down at 35 mm from a 35 mm diameter permanent magnet measured at (i) 52.3 K and (ii) 80.1 K. Reproduced from [109]. © IOP Publishing Ltd. All rights reserved. The blue (upper) and red (lower) lines are calculated with the mean field model detailed in sections 4.4.2.
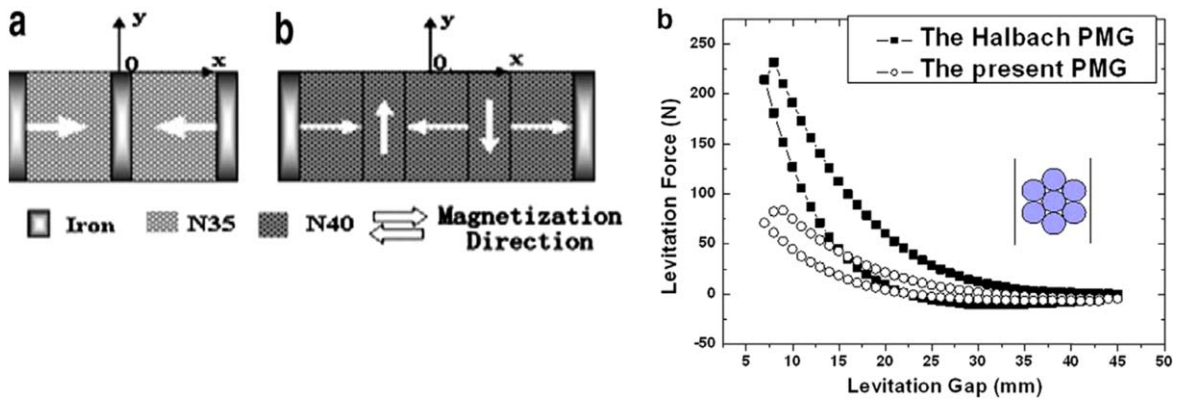

Figure 16. On the left: schemas of the arrays of magnets investigated by Jing *et al* [35]; N35 and N40 refer to NdFeB magnets with slightly different properties. On the right: the levitation forces between these guideways and the arrangement of seven superconductors shown in the figure. In their article the authors call 'present' and 'Halbach' the a and b arrays of magnets, respectively. Reprinted from [35], Copyright (2012), with permission from Elsevier.

entering or exiting the levitating vehicle and lateral ones from the curves along the guideway.

Liao *et al* [113] have investigated the static and dynamic relaxation of YBCO and GdBCO disks moving above a magnetic guideway at various velocities. The levitation force decreases as long as the superconductor is in motion but recovers a value not very different from that expected from static relaxation when the velocity is brought back to zero.
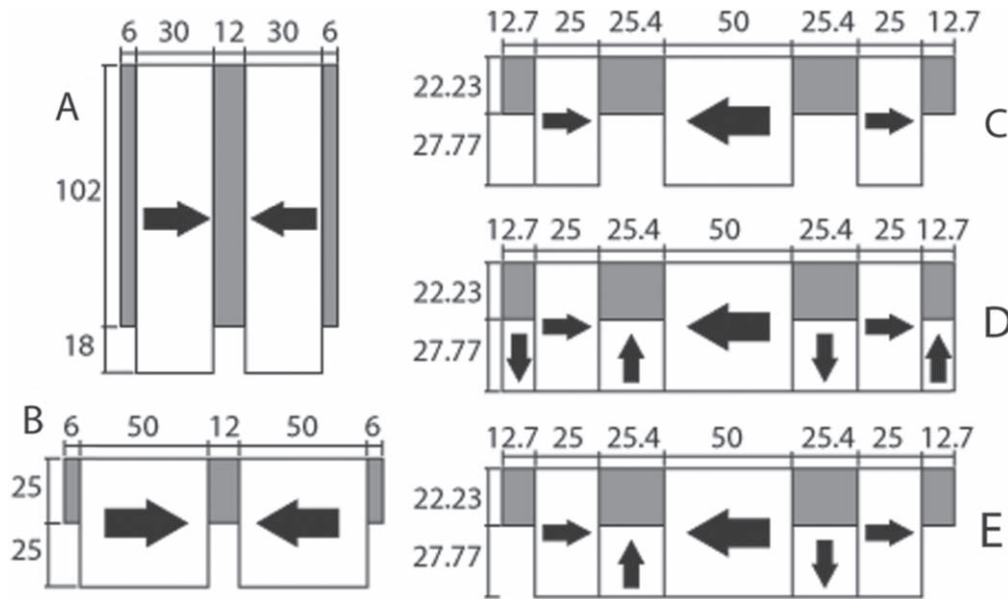
Figure 17. The five types of magnets and iron poles (in gray) arrangement investigated by Sotelo *et al* to determine the most suitable design for levitating the cryostats of the Maglev-Cobra. © 2010 IEEE. Reprinted, with permission, from [40].
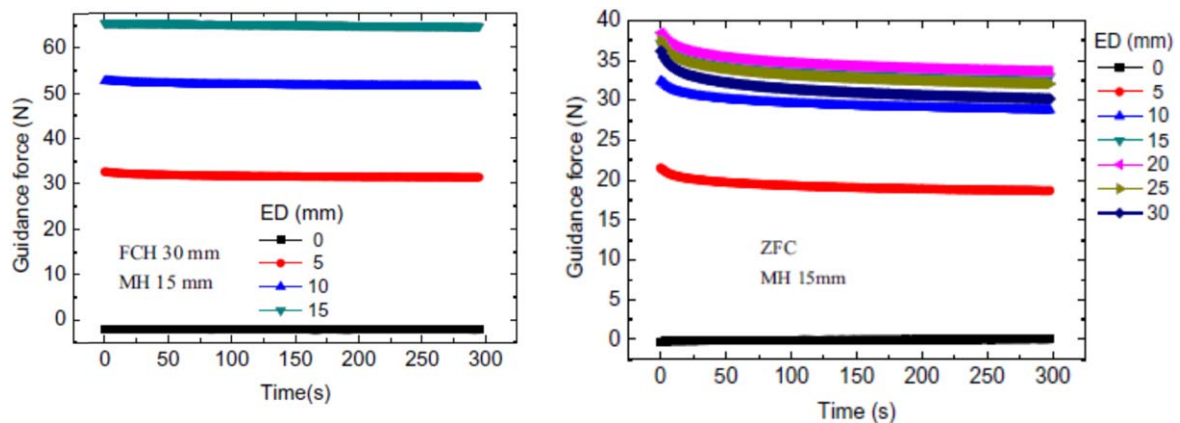

Figure 18. Modulation of the guidance force of an assembly of four three-seeded YBCO bulks levitating above a guideway as a function of time for various lateral displacements (ED). The guideway-superconductors separation (MH) was equal to 15 mm. On the left the superconductors were field cooled at distance $z_{cp} = 30$ mm from the guideway and ED increases from 0 to 15 mm from the bottom to the top of the figure. On the right they were zero field cooled and ED is equal to 0, 5, 10, 30, 25 and 20 mm from the bottom to the top of the figure. Reprinted by permission from Springer Nature Customer Service Centre GmbH: Springer, Journal of Superconductivity and Novel Magnetism, [15], © Springer Science+Business Media New York 2014.

The attenuation of the force, however, increases with the superconductor velocity. According to the authors, this can be attributed to more rapid fluctuations in the magnetic flux applied to the superconductor at high velocities.

Liu *et al* [114] have studied the effects of lateral displacements on the levitation force of YBCO disks levitating above various guideways. In all the cases they have found an appreciable decrease of the levitation force. Similar measurements in static conditions were carried out by Che *et al* [15] on an assembly of four ATZ three-seeded YBCO bulks levitating above a guideway. The levitation force decreased rapidly in the first few seconds following the lateral displacement, then much more slowly. If the superconductors were field cooled, the modulation of the levitation force by the amplitude of the displacement was opposite to

that observed in zero field cooling. In ZFC, the decrease of the levitation force was an increasing function of the displacement. In field cooling, the levitation force firstly decreased, then increased. The guidance force in FC was an increasing function of the amplitude of the displacement, while it showed a more complicated behaviour in zero field cooling. For the same displacement the guidance force in field cooling conditions was always larger than in zero field cooling. In addition, it decreased much more slowly along time after field cooling than after zero field cooling (see figure 18).

Dias *et al* [39] have investigated the effect along time of vibrations in the 1 Hz range and of repetitive vertical displacements on the levitating position of an ATZ cryostat. They have concluded that the decay of the levitation force
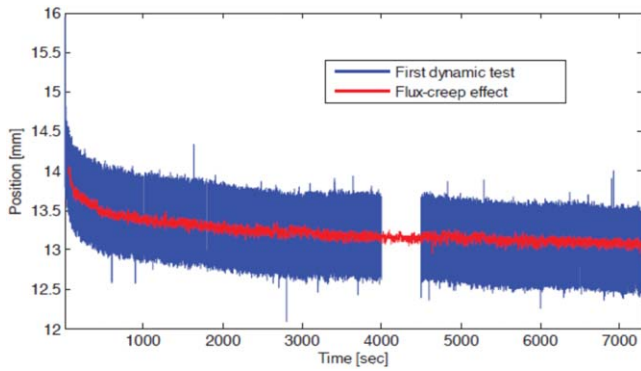
Figure 19. Decay of the levitation height of an ATZ cryostat including 24 three-seeded YBCO bulks measured with (blue line) and without (red line) applied vibrations. Reprinted from [39], Copyright (2012), with permission from Elsevier.

after vibrations were suppressed was similar to that observed when no vibrations or vertical displacements are applied (see figure 19). Yang *et al* [115] have shown that, as far as the amplitude of the vibrations is moderate, the levitation force does not depend on their frequency and that there is only a small increase of the hysteresis losses with frequency. These results suggest that, while thermal depinning results in the dissipation of the superconductor magnetic energy, vibrations or repetitive vertical displacements do not increase strongly the rate of dissipation.

4. A critical review of the models proposed for reproducing the levitation of superconductors: description and comparison to experimental results

Different analytical and numerical approaches have been proposed for modelling magnetic levitation. Analytical models require a regular distribution of the applied field and are practical with simple superconductor shapes with a high level of symmetry only. They have however the advantages to require much less computation time than numerical simulations and to show physical laws that are not always obvious in the results of simulations.

The most popular models solve differential Maxwell equations supposing that the relation between the electric field $\vec{E}$ and the current density $\vec{J}$ in the superconductor is a power law. Other works are based on the critical state model (CSM) and either energy minimization or magnetic moment calculations.

In the Bean description, the CSM supposes that the superconducting current density can only be equal to $-\vec{J_c}$, 0, or $+\vec{J_c}$. As a result, the $E(J)$ relation is undetermined and there is a discontinuity in the resistivity $\rho(J)$ of the superconductor that is not easily managed in numerical simulation [116]. As a consequence, for the calculation of losses one must first use the Maxwell equations (Faraday's law) to evaluate the electric field due to the variation of the magnetic field.

The generally used power law takes the form:

$$E = E_c \left(\frac{J}{J_c} \right)^n \tag{1}$$

where E_c is usually the electric field criterion employed for defining J_c, while n is proportional to the activation energy of vortex depinning. As a consequence, the power law is regarded as the mathematical expression of flux creep, that is responsible for magnetic relaxation. Numerical simulations with a power law are easier than with the CSM, the calculation of losses can be done with equation (1) and the Ohm's law and magnetic relaxation can be accounted for. As a result, the decreases of the levitation force and height as functions of time can be calculated. A detailed comparison of the advantages and disadvantages of the power law with respect to the CSM as well as a description of the problems encountered in the numerical modelling of superconductors can be found in [116].

In this section, we discuss some models solving Maxwell differential equations and we address those based on energy minimization and the calculation of magnetic moments. We underscore that when modelling concerns systems with either a cylindrical or a rectangular symmetry, the z-axis of the coordinate system is along the axis common to the superconductor and the permanent magnet. We begin with a model that does not take into account flux penetration in the superconductor. As a consequence, it provides the maximum force attainable with the investigated system, i.e. the Meissner limit. It also accounts for most of the characteristics of levitation mentioned in section 3.4.

4.1. The Badia–Freyhardt model [117]

The Badia–Freyhardt model is an analytical model that considers in ZFC the interaction between cylindrical magnets and superconductors with diameters d_{pm} and d_s, respectively. It supposes that the current flows on the superconductor surface facing the permanent magnet only. The authors write both the expressions of the component of the vector potential due to the superconducting current, $\overrightarrow{A_J}$ and that of the current density $\vec{J}$ with cylindrical functions. Then, they impose the following boundary conditions: (i) on the surface of the superconductor $\overrightarrow{A_J} = -\overrightarrow{A_M}$, where $\overrightarrow{A_M}$ is the component of the vector-potential due to the permanent magnet and (ii) the current density is equal to zero for $r > \frac{d_s}{2}$. They calculate the field on the surface of the superconductor. Using integral transforms, they solve exactly the resulting equations to obtain on the one hand the field generated by the superconducting currents and the current density on the surface of the superconductor on the other hand. They write the magnetic energy of the superconductor as the interaction energy between the current loops. The force of interaction between the superconductor and the permanent magnet is obtained by derivation of the magnetic energy.

This model accounts for the linear relationship between the levitation force and d_s^3 and the decrease of the levitation force for $d_{pm} > d_s$. It predicts that there is saturation of the

levitation force as the thickness of the permanent magnet increases. The levitation forces calculated with the model are much larger than those measured on YBCO samples when the magnet-superconductor separation is low, while there is a good agreement above some distance threshold. The discrepancies at low separation are due to the model not taking into account flux penetration, while the good agreement occurs for magnet fields lower than the superconductor first critical field.

4.2. Models based on the differential Maxwell equations and a power law for the current density

There are two main formulations for these models. Both formulations use equation (1) or a similar equation. The A-V formulation (A for vector potential and V for electric potential) is based on equations (2)–(4) between electric field $\vec{E}$, potential V, vector potential $\vec{A}$, magnetic field $\vec{B}$ and current density $\vec{J}$. The H-formulation (H for magnetic field) rests on equations (4) and (5) between $\vec{E}$, $\vec{J}$ and $\vec{H}$ [118]:

$$\vec{E} = -\frac{\partial \vec{A}}{\partial t} - \overline{\nabla V} \tag{2}$$

$$\vec{B} = \vec{\nabla} \times \vec{A} \tag{3}$$

$$\vec{J} = \frac{1}{\mu_0}\vec{\nabla} \times \vec{B} = \vec{\nabla} \times \vec{H} \tag{4}$$

$$\vec{\nabla} \times \vec{E} = -\mu_0\frac{\partial \vec{H}}{\partial t} \tag{5}$$

The interaction force between the permanent magnet and the superconductor is written as:

$$\vec{F} = \int_\nu \vec{J} \times \vec{B}d\nu. \tag{6}$$

In equation (6), the integration is carried out on the volume ν of the superconductor. Vector potential $\vec{A}$ and fields $\vec{B}$ and $\vec{H}$ consist of components $\vec{A}_M$, $\vec{B}_M$ and $\vec{H}_M$ resulting from the presence of the permanent magnet and $\vec{A}_J$, $\vec{B}_J$ and $\vec{H}_J$ due to the superconducting currents. For the numerical simulations, the relevant equations are combined to give the equation to be solved. It is generally:

$$\frac{\mu_0}{\rho} \cdot \frac{\partial \vec{A}}{\partial t} + \vec{\nabla} \times \vec{\nabla} \times \vec{A} = -\frac{\mu_0}{\rho}\vec{\nabla}V \tag{7}$$

for the A-V formulation and

$$\vec{\nabla} \times \rho\vec{\nabla} \times \vec{H} = -\frac{\partial \vec{H}}{\partial t} \tag{8}$$

for the H formulation. Resistivity ρ is calculated with $E = \rho J$ and equation (1).

4.2.1. Numerical simulations based on the H- formulation.
Sass et al [104] have considered both a bulk superconductor and a stack of coated conductors tapes [119] levitating above a permanent magnet. Here, we focus on the study of the bulk. Numerical simulations were carried out with the H-formulation. The authors present firstly an analytical method for evaluating field $\vec{H}_M$ as a function of the
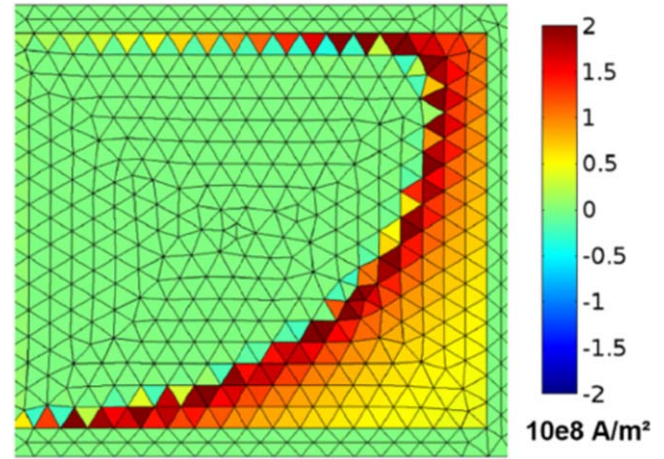

Figure 20. Current distribution in a half HTS bulk with dimensions 14 mm × 34 mm × 67 mm when it is 5 mm above a 50 mm × 50 mm × 100 mm NdFeB magnet after field cooling at $z_{cp} = 100$ mm according to the calculations by Sass et al. Reproduced from [104]. © IOP Publishing Ltd. CC BY 3.0.

permanent magnet magnetization. To take into account the dependency of the critical current density on the applied field, they add equations (9) and (10) to equations (1), (4) and (5):

$$J_c = J_{c0}.\exp\left(-\frac{|\vec{H}|}{H^*}\right) \tag{9}$$

$$n = n_0.\exp\left(-\frac{|\vec{H}|}{H_n}\right). \tag{10}$$

In equations (9) and (10), H^* and H_n are fitting parameters. The equations are solved in 2D by a finite element method (FEM). The permanent magnet and the superconductor having rectangular shapes, the levitation force per unit length is written in the Cartesian coordinate system (Oxyz) as:

$$\tilde{F}_Z = \int_{S_T} \mu_0 H_y(y, z, t).J_x(y, z, t)dS_T \tag{11}$$

where $dS_T = dydz$ is the differential cross section of the superconductor. According to the calculations, the current flows in the whole thickness of the bulk, although the penetrated area is much larger in the part facing the permanent magnet than in the opposite part (see figure 20). A good reproduction of measurements carried out at 77 K was obtained when setting H^* at a suitable value and the other fitting parameters in the range expected for YBCO at 77 K ($J_{c0} = 3.7 \times 10^8$ A cm^{-2} and $n = 21$).

Queval et al [118] have worked on the same systems—a stack of coated conductors tapes and a bulk superconductor levitating above a permanent magnet—as Sass et al. The simulations on the bulk were carried out with the H-formulation firstly in 2D, then in 3D. The authors did not use an analytical method for evaluating $\vec{H}_M$ but a FEM using the A-formulation. They have accounted for the modulation

of J_c by the magnetic field with the relation:

$$J_c(\vec{B}) = \frac{J_{c0}}{1 + \frac{|\vec{B}|}{B_0}} \qquad (12)$$

where B_0 is a material parameter. They have modified consistently the power law. The components of field $\vec{H}_J$ and the interaction forces were respectively calculated with the Biot-Savart law and equation (6). Measurements on the simulated set-up were carried out and the results compared to the calculations, using the same fitting parameters for the 2D and the 3D simulations. The J_{c0} and n fitting parameters were in the same range of magnitude as those of Sass *et al* Concerning the levitation force, 2D and 3D simulations reproduce the measurements with almost the same accuracy.

In additional experiments, the levitation and lateral forces were measured: (i) when the superconductor was cooled down off axis in ZFC and the permanent magnet motion was along the *z*-axis and (ii) when the superconductor was field cooled at 25 cm from the permanent magnet, the magnet-superconductor separation reduced to 5 cm and the magnet moved along the *y*-axis. These measurements were simulated in 3D.

The calculated levitation and lateral forces after off-axis cooling were in a fair agreement with the measurements. During the lateral motion of the permanent magnet, the calculated levitation forces were very near the measurements, while the calculation of the lateral forces was less accurate. The simulations have reproduced the instability of the permanent magnet above the superconductor shown by the measurements. According to the authors the cause of the discrepancies is that they have not taken into account the anisotropy of the critical current density in cuprates.

4.2.2. Numerical simulations based on the A-V formulation.
Ma *et al* [37] have used the A-V formulation (equation (7)) to describe in 2D the mutual effects of three bulk superconductors located above two different types of Halbach guideways (see figure 21). They did not use a power law for the current density but an equivalent relation based on the Bean–Kim model of the critical state that accounts also for the effect of the applied field [36, 37]:

$$J = J_{c0} \left(\frac{B_0}{|\vec{B}| + B_0} \right) \tanh \left(\frac{E}{E_c} \right). \qquad (13)$$

In equation (13), J_{c0} is the critical current density when no field is applied. The B_0 selected for the simulations was in the same range of magnitude as the B_0 used by Queval *et al* [118]. The field generated by the Halbach arrays was determined analytically. Equation (6) was used for the determination of the components of the force resulting from the interaction of the current in each bulk with the field generated by the magnets as well as by the other bulks. Although the total levitation force is probably overestimated, it is in the range of the forces measured with three-seeded bulks, supporting the validity of the technique. The magnetic interaction between bulks has proved to have little effects on
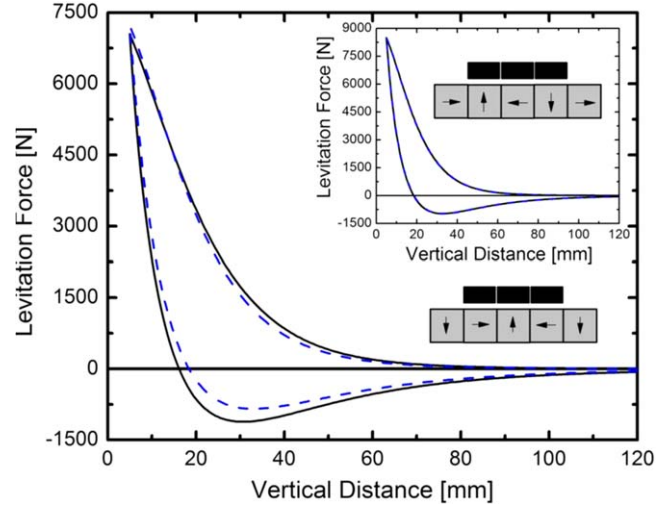

Figure 21. Levitation force per unit length of a system consisting of three bulks levitating above two different Halbach arrays calculated by Ma *et al* [36]. The dashed line reports the calculation carried out while neglecting the magnetic interactions between bulks. Reprinted from [36], with the permission of AIP Publishing.

the levitation force, the distribution of the magnetic field and that of the induced current. The calculations have also shown that there is in each bulk regions free of field and current and that the currents loops are mainly located in the part of the bulks facing the Halbach arrays.

With the same technique the authors have, in another paper, compared the performances above the same Halbach arrays of (i) a single bulk and (ii) sets of bulks with the same total surface as the single one comprising $N = 2$, $N = 4$ and $N = 8$ pieces [38]. The calculations have shown that the levitation force tends to decrease as N increases, as does the surface of the current loops. While the same result was obtained for the guidance force above one Halbach array, the situation was more complex above the other one, the guidance force being larger for $N = 2$, 4 and 8 than for $N = 1$. The Ma *et al* simulations have not taken into account the inter-grain current flowing in three-seeded bulks. The authors have considered the intra-grain currents only. This work shows however the capability of the simulations techniques to model operational levitation set ups.

4.2.3. The Qin–Li–Liu–Dou–Brandt numerical model [111].
This model is a variant of the A-V formulation. The authors consider cylindrical magnets and superconductors in ZFC. From the London gauge:

$$\vec{\nabla}.\vec{A}_J = 0 \qquad (14)$$

and the Laplace equation:

$$\mu_0 \vec{J} = -\nabla^2 \vec{A}_J \qquad (15)$$

they write the integral form of $A_J(r,z)$ as a function of $J(r,z)$. From this expression and equation (2), taking V as a constant, they write the integral form of field $E(r,z)$ as a function of $\frac{\partial J}{\partial t}(r, z)$. Inversing this relation they obtain $\frac{\partial J}{\partial t}$ as a function of $E(r,z)$, that is given the form in equation (1). Current density J

(r,z) is numerically integrated writing:

$$J(r, z, t + dt) = J(r, z, t) + \frac{\partial J(r, z, t)}{\partial t} dt \qquad (16)$$

starting with $J(r, z, t) = 0$. The levitation force is calculated with equation (6). The field and current distribution in the superconductor as well as the levitation force are calculated as functions of the superconductor dimensions, the rate of change of the magnet-superconductor separation, $B_M(r, z)$, J_c and exponent n. The saturation of the levitation force observed for large J_c is due to ideal magnetic screening i.e. corresponds to the Meissner limit. Otherwise, the stronger the current density, the narrower the hysteresis loops, consistently with the results reported in section 3.4.3. For low n values, the model accounts for the decrease of the levitation force in the near proximity of the permanent magnet that can occur in the vicinity of T_c, mentioned in section 3.4.3. For the authors, the asymmetry of the magnetization loops results from the saturation of the superconductor magnetic moment when the permanent magnet is moving toward the superconductor and is close to it, while it is not saturated when the magnet is moving away. The decay along time of the levitation force is found to follow a $F_Z \propto t^{-\frac{1}{n-1}}$ law. Otherwise, the model predicts that F_Z depends on the rate of change of the magnet-superconductor separation. As a consequence, the levitation force should depend on the frequency of vibrations. This is not consistent with the observations reported in section 3.4.5. However, the calculations were achieved with a low n value not well suited to YBCO and (RE)BCO bulks at 77 K and could be different for larger n.

4.2.3.1. Conclusions on the numerical simulations methods.
Some authors have repeated the simulations reported in section 4.2.2 using a modified A-V formulation instead of the H one [102]. They have concluded that both techniques bring similar results, confirming that both the A-V and H-formulations of the differential Maxwell equations result in a good reproduction of the measurements if they are associated with suitable $E(J)$ and $J_c(B)$ relations. As long as it avoids a mathematical discontinuity, the selected $E[J(B)]$ function has little effect on the validity of the results. Simulations with either equations (1), (9) and (10) or equations (1) and (12) or equation (13) give good results. Authors have taken advantage of the capability of the FEMs to mesh complex shapes for carrying out the simulation of realistic SML bearings demonstrating their utility for further developments of SML systems.

4.3. Models based on the minimization of the magnetic energy

The Barcelona group has proposed a CSM model that determines the levitating and the guidance forces by minimization of the magnetic energy. Considering a cylindrical system consisting of a permanent magnet and a ZFC superconductor, the authors have modelled in 2D the superconductor as current carrying coaxial rings with a rectangular section [120, 121]. The magnetic energy of the superconductor was set equal to the mutual energy of the current

lines. The authors have determined the current distribution that minimizes the magnetic energy and calculated the levitation force during the motion of the permanent magnet with an expression derived from equation (6).

According to the results, the hysteresis is due to the existence of two current layers flowing in opposite directions during the ascending stage of the superconductor, while a single layer exists in the descending stage [120]. In addition, the superconductor can be not completely penetrated by the currents and the levitation force tends towards saturation i.e. the Meissner limit as T decreases and J_c increases [110]. Comparing the force obtained in ZFC to that measured in the same conditions when the superconductor is field cooled, they conclude that while the levitation force is larger in ZFC than in FC, the guidance stiffness is generally larger in FC than in ZFC. These results are consistent with the observations reported in section 3.4.1. The predicted behaviour of the levitation force, as a function of d_s/d_{pm} is similar to the results reported in section 3.4.2, the largest force occurring for $d_s = d_{pm}$.

For the simulation in 2D of the hysteresis loops of rectangular superconductors in interaction with either rectangular magnets or Halbach arrays, the authors have considered infinitely long superconductors and magnets. They have written the functional of equation (17) that accounts for the magnetic energy of the superconductor at a given permanent magnet-superconductor separation [123]:

$$\mathcal{F}[J] = \frac{1}{2} \int_S J(r) A_J(r) dS - \int_S J(r) \hat{A}_J(r) dS$$
$$+ \int_S J(r) [A_M(r) - \hat{A}_M(r)] dS. \qquad (17)$$

In equation (17), S is the superconductor cross section. The quantities with hat correspond to the previous magnet–superconductor separation i.e. at the previous time layer. Since the superconducting current distribution minimizes $\mathcal{F}[J]$ [124–126], the authors write the relation between A_J and J to determine this distribution. They calculate the levitation force per unit length of the superconductor with equation (6).

For magnets and superconductors with width a_{pm} and a, respectively, the authors claim that the maximum force is obtained for $\frac{a_{pm}}{a} \sim 0.7$ [122], that is different from the results obtained with cylindrical superconductors and magnets. They have investigated the dependency of the levitation force on the thickness of the magnets and found results qualitatively in agreement with those reported in section 3.4.2. They have also investigated the levitation force and guidance stiffness, damping and minor hysteresis cycles of superconductors interacting with various magnets arrays as functions of the magnets dimensions and locations [112, 122, 127]. They have evaluated the benefits of adding a soft magnetic yoke to a system consisting of two permanent magnets with opposite horizontal magnetization and determined the dimensions of the yoke optimizing the levitation force [128]. Investigating the decrease of the levitation force when the superconductor is repetitively laterally displaced above the magnets [129] they have calculated forces very similar to the measurements
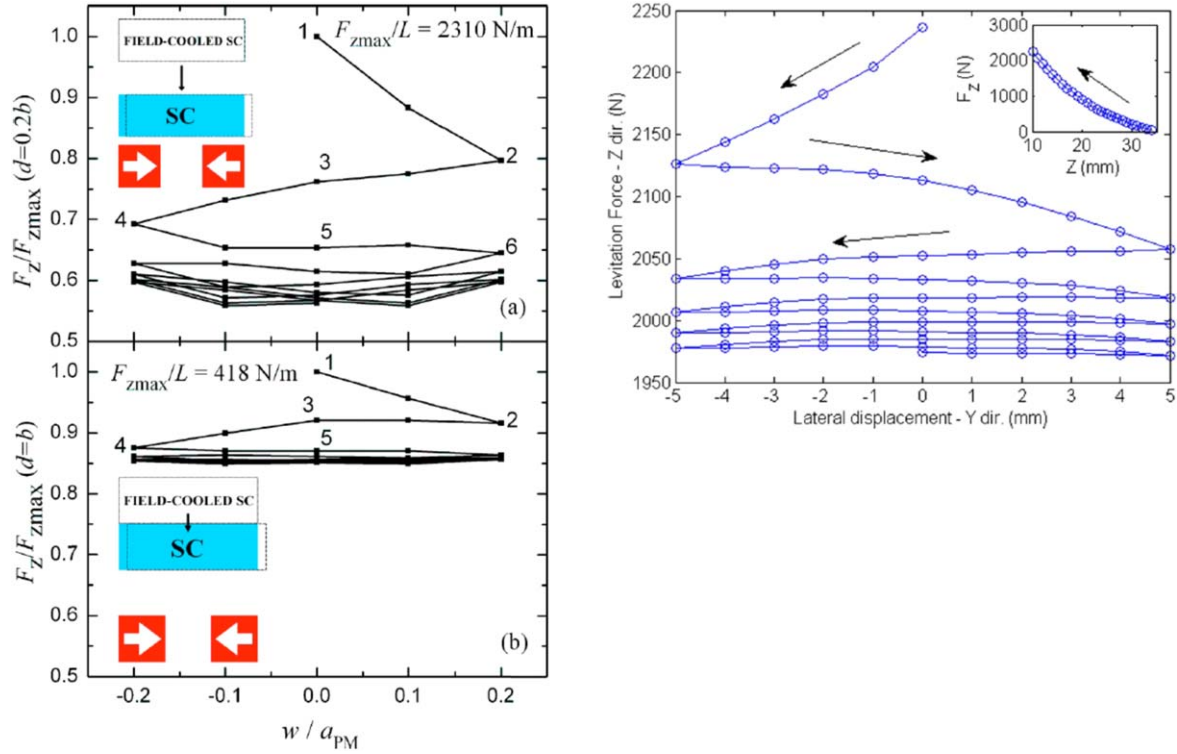
Figure 22. Decrease in the levitation force when a superconductor (SC) is repetitively laterally displaced above the magnets shown in the figure calculated by Del Valle *et al* (Reprinted from[129], with the permission of AIP Publishing) on the left and results of measurements carried out in similar conditions on a cryostat containing 24 three-seeded bulks above an Halbach guideway by Sotelo *et al* (© 2010 IEEE. Reprinted, with permission, from [42]) on the right.

carried out later by the Rio group under similar conditions (see figure 22) [42].

4.3.1. Conclusions regarding the models based on the minimization of the magnetic energy.
The models based on the minimization of the magnetic energy account, at least qualitatively, for almost all the features of magnetic levitation described in section 3.4. However, only 2D simulations could be carried out, the simulated systems being either cylindrical or infinite in the current direction.

4.4. Models based on the calculation of magnetic moments

4.4.1. The magnetic image model.
The magnetic image model is based on the CSM. Initially the permanent magnet is at location $\vec{r}_0$ (x_0, y_0, z_0), the origin of the axis being taken on the superconductor surface. During field cooling the magnetic moment of the permanent magnet, $\vec{m}(\vec{r}_0)$, generates a 'frozen' symmetrical image moment with respect to the superconductor surface [130]. The normal component of the field created at the surface of the superconductor by the frozen moment is equal to that generated by the permanent magnet moment. The total field at the surface of the superconductor must not change when the location or the orientation of the magnet changes. If the permanent magnet is displaced from $\vec{r}_0$ to $\vec{r}_1(x_1,y_1,z_1)$, an image of the magnet moment $\vec{m}(\vec{r}_1)$ is

generated in order that:

$$B_{Z_{PM}}(x_1, y_1, z_1) + B_{Z_{im}}(x_1, y_1, -z_1) = 0. \qquad (18)$$

In equation (18), $B_{Z_{PM}}(x_1, y_1, z_1)$ and $B_{Z_{im}}(x_1, y_1, -z_1)$ are the normal component of the field generated at the surface of the superconductor by the magnet moment and the image moment respectively. As a result, the interaction between the permanent magnet and the shielding currents flowing in the superconductor is described as the interaction of the permanent magnet with the field $\vec{B}_{im}(\vec{r})$ generated by the images of $\vec{m}(\vec{r}_0)$ and $\vec{m}(\vec{r}_1)$. The fields inside and outside the superconductor take respectively the form of equations (19) and (20):

$$\vec{B}(x, y, z) = \vec{B}_{PM}(x - x_0, \ y - y_0, \ z - z_0) \qquad (19)$$

$$\vec{B}(x, y, z) = \vec{B}_{PM}(x - x_0, \ y - y_0, \ z - z_0) + \vec{B}_{im}(x, y, z). \qquad (20)$$

If the permanent magnet is located in $\vec{r}_1$ the interaction force is written as:

$$\vec{F}(\vec{r}_1) = [\vec{m}(\vec{r}_1) \cdot \vec{\nabla}] \vec{B}_{im}(\vec{r}_1). \qquad (21)$$

Considering a cylindrical permanent magnet and superconductor, Hull and Cansiz [131] have modelled the permanent magnet and its image as amperian current loops. In this case, they have used the expression of the force
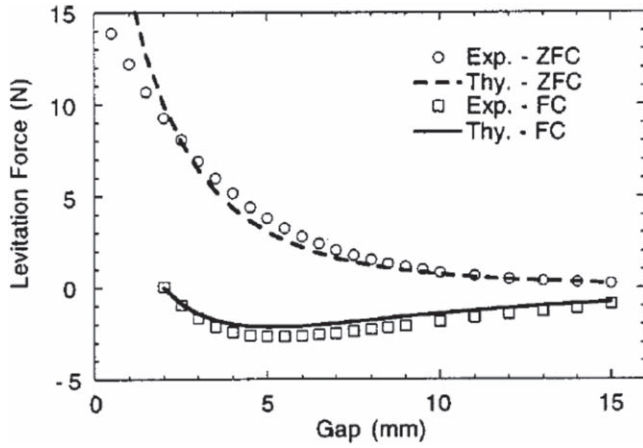
Figure 23. Comparison between the levitation forces calculated by Hull and Cansiz in FC and ZFC, and the measurements. Reprinted from [131], with the permission of AIP Publishing.

between two current loops in the axisymmetric case to calculate the levitation force. With no free parameters, they have obtained a good agreement with the measurements (see figure 23). In the form presented here, the magnetic image model can reproduce the descending step of the hysteresis loop in figure 8 only. To remedy this problem, Yang and Chen have proposed to introduce an additional moment they called m_4 accounting for both the flux trapped in the superconductor when the motion of the permanent magnet is reversed and the flux change due to the ascending motion of the permanent magnet [132]. Wu et al have shown that the modified model results at least in a qualitative agreement with measured hysteresis cycles [133]. An advantage of the magnetic images model is that, with suitable changes, it can account for lateral displacements as well as for vertical ones [131]. It allows the calculation of the forces and torques between the superconductor and the permanent magnet, even if their surfaces are not parallel. This is the reason why, considering the possible use of the magnet-superconductor interactions for the docking of two spacecrafts, some authors have selected the magnetic images for modelling this process [134, 135]. However, the model supposes that the shielding currents in the superconductor can generate images of the magnet moment, whatever the size or the critical current density of the bulk, although real superconductors have limited dimensions and critical current density. For carrying out more exact calculations, the magnet should be modelled not as a single but as a set of magnetic dipoles [111], that would make the calculations much more complicated. As a consequence, the levitation forces calculated according to the procedure described above are often overestimated. Otherwise, the calculations require a large number of free parameters and can involve the numerical integration of functions. As a result, it is difficult with this model to account for the characteristics of levitation described in section 3.4.

4.4.2. The mean field model. The mean field model [109, 136] is an analytical model based on the CSM developed for systems with the cylindrical symmetry of

figure 8 and $d_{pm} \geqslant d_s$. It is based on the following aspects of the physics of FC type II superconductors mentioned in section 2.3: (i) no shielding current but pinned vortices are induced during field cooling and (ii) the generation of shielding current aims at restoring the field that existed during field cooling. An additional hypothesis is that the shielding currents flow in one or several superimposed layers with thickness t facing the magnet, as suggested by Navau et al [120]. The determination of the levitation force is based on the observation by Sanchez et al [123] that if the field and the field gradient can be regarded as constants in the superconductor and functions of separation z only, the levitation force can be written as:

$$F_z(z) = m_z \frac{\partial B_{Z_{PM}}}{\partial z}. \tag{22}$$

In equation (22), $B_{Z_{PM}}$ is the vertical component of the magnet field along the axis common to the permanent magnet and the superconductor and m_z the magnetic moment of the currents flowing in the superconductor. Equation (22) has a form similar to equation (21) of the magnetic images model. However, the field and the field gradient generated by the permanent magnet are nonuniform on the scale of the thickness h_s of a bulk. For extending the validity of equation (22) to bulk samples, $\frac{\partial B_{Z_{PM}}}{\partial z}$ is replaced by $\frac{\partial B^*_{Z_{PM}}(z)}{\partial z}$ that is either its mean value on thickness t or the midrange value $\frac{1}{2}\left(\frac{\partial B_{Z_{PM}}(z)}{\partial z} + \frac{\partial B_{Z_{PM}}(z+t)}{\partial z}\right)$. Calculations with the two quantities give almost the same results. The magnetic moment m_z is written according to the expression proposed by Brandt for the magnetic moment of a disk in a uniform axial field B [137]:

$$m_z = -\frac{2}{3} J_c t R^3 \left[\cos^{-1}\left(\frac{1}{\cosh\left(\frac{2B}{\mu_0 J_c t}\right)} \right) + \frac{\sinh \left| \frac{2B}{\mu_0 J_c t} \right|}{\cosh^2\left(\frac{2B}{\mu_0 J_c t}\right)} \right]. \tag{23}$$

During the descending step of the magnet in figure 8, the shielding currents are supposed to flow in a single layer. Magnetic field B in equation (23) is replaced by:

$$\Delta B_a = B^*(z) - B^*(z_{cp}) \tag{24}$$

and J_c by J_p, the current density in the current carrying layer. In equation (24), $B^*(z)$ is the midrange or the mean value on thickness t of the magnet field at distance z along the axis of the superconductor and $B^*(z_{cp})$ that at the cooling point z_{cp}. Current density J_p, is related to J_c by:

$$J_c = J_p . \frac{t}{h_s}. \tag{25}$$

The levitation force is calculated inserting the resulting moment m_{down} and $\frac{\partial B^*_{Z_{PM}}(z)}{\partial z}$ in equation (22). After the magnet motion is reversed at z_{min}, the shielding currents present in the superconductor do not disappear. Since they
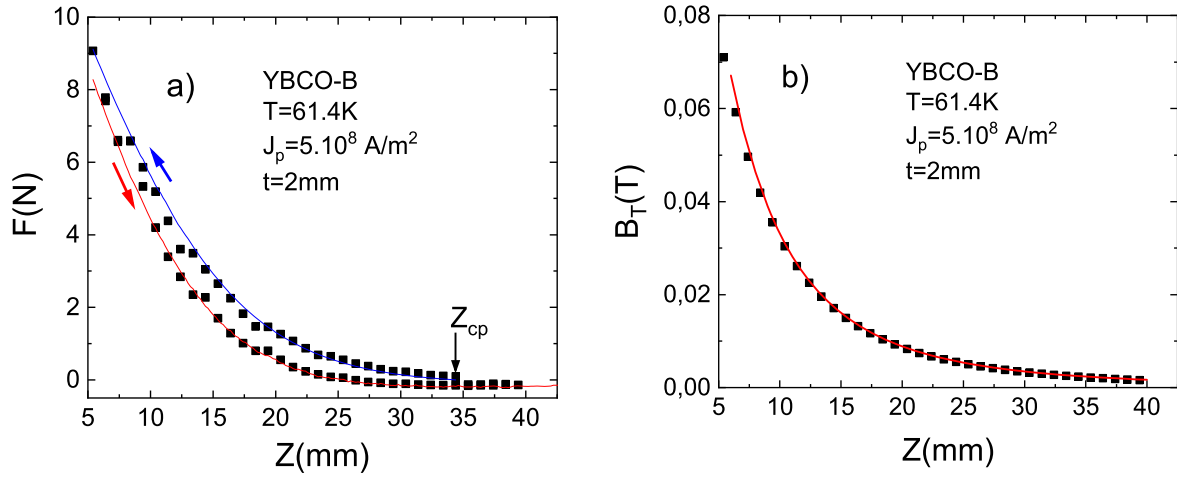
Figure 24. (a) Hysteresis cycle of the vertical interaction force between a 18.6 mm diameter 11.4 mm thick YBCO cylinder at 61.4 K and a 45 mm diameter NdFeB permanent magnet [138]; (b) Field trapped in the same sample at the same temperature. The dots are the measurements; the ascending (blue) and descending (red) lines in figure 23(a) are calculated with the J_p and t indicated in the figure and equations (22) and (26), respectively. The continuous line in figure 23(b) is calculated inserting the same J_p and t in the Chen *et al* relation [139] supposing that the current flows with density J_p in a layer with thickness t located in the middle of the bulk. Reproduced from [139]. © IOP Publishing Ltd. All rights reserved.

can't restore the field existing during field cooling at $z \neq z_{min}$, the model supposes that an additional current carrying layer with thickness t and current density $-J_p$ superimposed to the first one is generated in the sample, that involves $t \leqslant \frac{h_s}{2}$ as a consequence. The magnetic moment comprises two components $m_{max}(\Delta B_{max})$ and $m_r(\Delta B_r)$, where $\Delta B_{max} = B^*(z_{min}) - B^*(z_{cp})$ and $\Delta B_r = B^*(z) - B^*(z_{min})$ replace B in equation (23). The current flowing in opposite directions in the two layers, m_{max} and m_r, have opposite signs. The levitation force during the upward motion of the magnet takes the form:

$$F_z = m_{max} \frac{\partial B^*_{PM}(z+t)}{\partial z} + m_r \frac{\partial B^*_{PM}(z)}{\partial z}. \qquad (26)$$

The hysteresis loops are reproduced with equations (22) and (26) taking t and J_p as free parameters. The validity of the procedure is confirmed by the reproduction of the trapped field measured on the same samples at the same temperature [138] with the Chen *et al* relation [139] supposing that the current flows with density J_p in a layer of thickness t located in the middle of the bulk (see figure 24). Current densities J_p and J_c can be determined from the force measurements, but in a limited range of temperature only, because of the saturation of F_z as the temperature decreases mentioned in section 3.4.3. The saturation of F_z results from that of m_z in equation (23) as J_c increases (see figure 14). Thickness t decreases as the temperature decreases. This behavior is addressed by considerations on the magnetic energy of the bulk that result in $t \propto J_p^{-\frac{2}{3}}$ [138]. The F_z saturation and the t decrease are consistent with the suggestion that F_z tends towards the Meissner limit as J_c increases. The closure of the hysteresis cycles as the temperature decreases is attributed to the little difference for small t between $\frac{\partial B^*_{PM}(z)}{\partial z}$ and $\frac{\partial B^*_{PM}(z+t)}{\partial z}$ on the one hand and m_{down} and $m_{max} + m_r$ on the other hand. Otherwise

the increase of F_z as the cooling height increases is ascribed to that of both ΔB_a and m_{down}. Finally, the $F_z \propto d_s^3$ measurements reported in section 3.4.2 are in agreement with the expression of m_z in equation (23).

4.4.2.1. Conclusions regarding the models based on the calculation of magnetic moments. Both the magnetic image model and the mean field model are based on the critical state model. In the magnetic image model the moment of the image due to the currents flowing in the sample during the descending motion of the magnet is similar to m_{down}, while moment m_4 introduced by Yang and Chen [132] is similar to $m_{max} + m_r$. The main differences between the models are: (i) the introduction of a 'frozen' moment during field cooling in the magnetic images model, while the mean field model considers that the field cooled magnetization of the superconductor consists in the entry and the pinning of vortices with no generation of shielding currents; (ii) the fact that the 'non-frozen' image moments are mobile in the superconductor while the current layers are facing the permanent magnet in the mean field model and (iii) the use of equation (23) in the mean field model for the calculation of the magnetic moments.

The magnetic image model is versatile and the modelling of various magnets and superconductors configurations is possible. Regarding disadvantages, it requires a large number of free parameters and can result in an inaccurate estimation of the interaction forces.

The mean field model is based on the physics of superconductors and account for many of the experimental results of section 3.4. It requires the measurement of $B(z)$ along the magnet axis only, discarding the variations of the applied field on the surface of the superconductor due to the divergence of the flux lines. The other models require the determination of $B(z)$ in a large volume. The predicted J_p, J_c and t are confirmed by trapped field measurements. However,
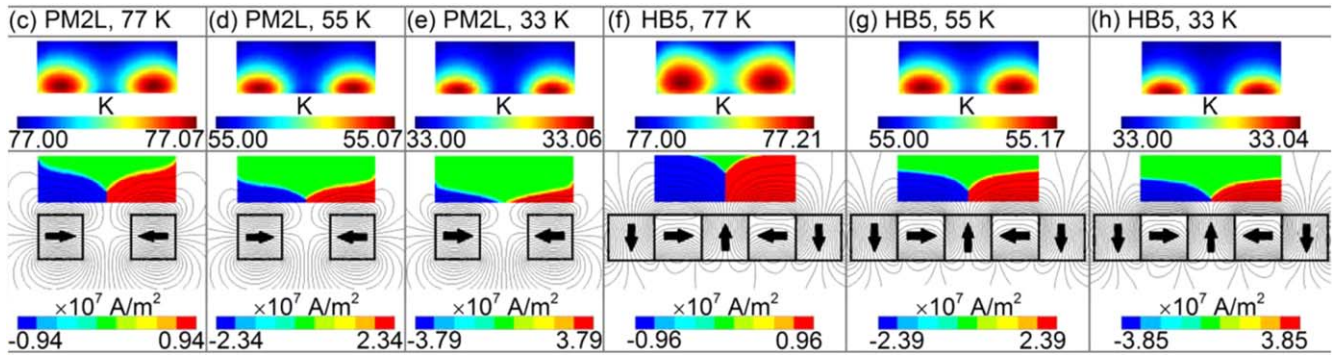
Figure 25. Temperature, current and field profiles in a HTS bulk levitating above two different guideways at various temperatures calculated by Huang *et al* with the A-V formulation of the Maxwell differential equations, taking into account the dependency of J_c on the temperature. Reproduced from [140]. © IOP Publishing Ltd. All rights reserved.

up to now, the model has described cylindrical axisymmetric systems only and was not extended for either describing other systems, rectangular magnets and superconductors, for example, or calculating the guidance force or describing multiple up and down motions of the permanent magnet.

4.5. Conclusions regarding the models proposed for reproducing the levitation of superconductors

The results obtained with power law models can show some differences to those obtained with the models based on the CSM. The models based on the CSM allow the existence of both a free boundary between the penetrated and the non-penetrated regions and several superimposed layers with opposite current directions. The location of the boundary is obtained as the result of the calculations. Its existence is consistent with the saturation of the levitating force at the Meissner limit at low temperature. It is supported by measurements carried out on two MgB_2 samples with different thicknesses fabricated in the same conditions that have resulted in identical force hysteresis loops [136]. Calculations with power law models result generally in currents distributed along the whole thickness of the superconductor and no superimposed current layers. However, inserting a $J_c(T)$ relation in the model in addition to the power law, A-V simulations by Huang *et al* of a rectangular superconductor levitating above two different guideways [140] have resulted in a more and more pronounced localisation of the current in the part of the superconductor facing the guideway as the temperature decreases (see figure 25). These results show that power law and CSM models can coincide for large J_c and n.

As a general rule, except the magnetic images models, the models based on the CSM have pronounced analytical features yielding predictions on the properties of magnetic levitation consistent with those detailed in section 3.4. The reproduction of the measurements can yield important material parameters, especially the critical current density. Power law models have the advantage to allow one to apply FEM modelling to 3D systems and set-ups that are neither symmetric nor axisymmetric. As a consequence, they are well suited for modelling operational SML systems. However, J_c is generally introduced in the calculations as an input among other free parameters and, as a consequence, is not determined univocally.

5. Conclusions and perspectives regarding SML systems

The feasibility of transportation systems based on SML was demonstrated by the Maglev-Cobra in Rio de Janeiro in Brazil. Levitation is due to the interaction between NdFeB magnets and bulk superconductors, the fabrication of which is mastered. As seen in section 4, the simulation techniques that have been developed can reproduce the forces between magnets and superconductors with complex shapes. They were often developed by the teams designing SML systems [35, 36, 40, 104]. They can be used for the design of optimized guideways and to predict the behaviour of a levitating train in operational conditions. New cryostats that can carry 5000 N are now available [141]. They could provide the force required for levitating light trains. Otherwise, investigations combining superconducting magnetic levitation for stability and magnet–magnet repulsion for increasing the levitation force are in progress [142]. From this point of view, since they can be fabricated in large pieces while the levitation force increases with d_s^3, MgB_2 superconductors could advantageously replace YBCO and (RE)BCO bulks. This would require either the replacement of liquid nitrogen by another cryogenic fluid such as H_2 or He or the implementation of cryogenerators. However, some technological breakthroughs must be achieved before SML transportation systems present decisive advantages as compared to EML ones. The most important is the development of fast static switch points at the scale of real vehicles and guideways that are 100% reliable. First results in this field have been published [18, 25]. Other obstacles to the development of the technology are the costs of both the magnets and the superconducting bulks. Authors have proposed solutions for reducing them. Deng *et al* [16], for example, have suggested an arrangement of the superconductors taking advantage of the anisotropy of YBCO and (RE)BCO bulks for optimizing the levitation and the guidance forces. This could lead to the construction of simplified guideways requiring fewer magnets

than classical ones. Coils consisting of coated conductor tapes could be an interesting alternative to HTS bulks. Unfortunately, no soldering technology insuring a perfect superconducting joint between the two ends of the tape and zero resistance to the coils has been developed yet, in spite of ingenious suggestions for circumventing the difficulty [143]. As mentioned in section 4 [104, 118], investigations into the possibility of replacing YBCO and (RE)BCO bulks with stacked coated conductor pieces have been carried out and brought promising results [144, 145]. Finally, for the sake of safety and maintenance, the decrease of the levitation and guidance forces and the resulting changes in the levitating height and location of the trains with respect to the guideway must be fully characterized in conditions similar to those of operational trains. If the developments in these different fields are successful, SML transportation systems could be attractive enough to persuade the railway industry to develop them.

Acknowledgments

ORCID iDs

P Bernstein ⓘ https://orcid.org/0000-0002-8104-2151
J Noudem ⓘ https://orcid.org/0000-0002-8020-9095

References

[1] Becker W 1966 The turbomolecular pump, its design, operation and theory; calculation of the pumping speed for various gases and their dependence on the forepump *Vacuum* **16** 62

[2] https://pfeiffer-vacuum.com

[3] Meslin E H *et al* 2009 Magnetic Bearings—Theory *Design and Application to Rotating Machinery* (Berlin: Springer) (https://doi.org/10.1007/978-3-642-00497-1)

[4] Geim A K *et al* 1999 Magnet levitation at your fingertips *Nature* **400** 323

[5] Simon M D and Geim A K 2000 Diamagnetic levitation: flying frogs and floating magnets *J. Appl. Phys.* **87** 6200

[6] Earnshaw S 1842 On the nature of the molecular forces which regulate the constitution of the luminiferous ether *Trans. Cambridge Philos. Soc.* **7** 97

[7] https://skf.com/binary/57-261934/Vernon_S2M.pdf

[8] Meins J *et al* 1988 The high speed Maglev transport system TRANSRAPID *IEEE Trans. Magn.* **24** 808

[9] Brandt E H 1988 Friction in Levitated Superconductors *Appl. Phys. Lett.* **53** 1554

[10] Lin Q X *et al* 2015 Measurement and calculation method of the radial stiffness of radial high-temperature superconducting bearings *J. Supercond. Nov. Magn.* **28** 1681

[11] Xu K X *et al* 2016 A fully superconducting bearing system for flywheel applications *Supercond. Sci. Technol.* **29** 064001

[12] Morandi A *et al* 2011 Numerical analysis and experimental measurements of magnetic bearings based on MgB_2 hollow cylinders *IEEE TAS* **21** 1460

[13] Walter H *et al* 2006 First heavy load bearing for industrial application with shaft loads up to 10 kN *J. Phys. Conf. Ser.* **43** 995

[14] Wang J *et al* 2002 The first man-loading high temperature superconducting Maglev test vehicle in the world *Physica* C **378–381** 809

[15] Che T *et al* 2014 Enhanced maglev performance by field cooling for HTS maglev system in curve negotiation *J. Supercond. Nov. Magn.* **27** 2211

[16] Deng Z *et al* 2013 An efficient and economical way to enhance the performance of present HTS Maglev systems by utilizing the anisotropy property of bulk superconductors *Supercond. Sci. Technol.* **26** 025001

[17] Deng Z *et al* 2007 Free vibration of the high temperature superconducting Maglev vehicle model *IEEE Trans. Appl. Supercond.* **17** 20171

[18] Li Y J *et al* 2016 Design and analysis of an electromagnetic turnout for the superconducting Maglev system *Physica C* **528** 84

[19] Rosenzweiga S *et al* 2012 A superconducting levitation transport model system for dynamical and didactical studies *Phys. Proc.* **36** 1037

[20] Jiasu S *et al* 2005 Design consideration of a high temperature superconductor Maglev vehicle system *IEEE Trans. Appl. Supercond.* **15** 2273

[21] Xu Y Y *et al* 2014 Dynamic response characteristics of a high-temperature superconducting Maglev vehicle under laterally unbalanced load conditions *J. Supercond. Nov. Magn.* **27** 35

[22] Yang W *et al* 2008 Hysteresis force loss and damping properties in a practical magnet–superconductor maglev test vehicle *Supercond. Sci. Technol.* **21** 015014

[23] Zeng R *et al* 2012 The influence on levitation force of the bulk HTSC above a permanent magnet guideway operating dive-lift movement with different angles *J. Supercond. Nov. Magn.* **25** 2309

[24] Yildizer I *et al* 2016 Optimization of levitation and guidance forces in a superconducting Maglev system *Cryogenics* **78** 57

[25] Liu X *et al* 2020 Magnetic field test on an electromagnetic turnout prototype system for high-Tc superconducting Maglev *IEEE Trans. Appl. Supercond.* **30** 3600206

[26] Stephan R *et al* 2017 Superconducting levitation applied to urban transportation *Wiley Encyclopedia of Electrical and Electronics Engineering* (https://doi.org/10.1002/047134608X.W8346)

[27] Lin G and Sheng X 2018 Application and further development of Maglev transportation in China *Transport. Syst. Technol.* **4** 36

[28] Information from the International Maglev Board—October 2019

[29] Shin B C *et al* 2011 Recent progress of urban maglev program in Korea *The 21st Int. Conf. on Magnetically Levitated Systems and Linear Drives (October 10–13, 2011) (Daejeon, Korea*

[30] Tandan G K 2015 A review on development and analysis of maglev train *Int. J. Res. Advent Technol.* **3** 14

[31] Post R 2004 Magnetically levitated trains takes flight *Sci. Technol. October* 2004

[32] Santangelo A 2018 Hyperloop as an evolution of Maglev *Transport. Syst. Technol.* **4** 44

[33] Wang S *et al* 2007 An update high-temperature superconducting maglev measurement system *IEEE TAS* **17** 2067

[34] Wang J *et al* 2007 Laboratory-scale high temperature superconducting Maglev launch system *IEEE TAS* **17** 2091

[35] Jing H, Wang J, Wang S, Wang L, Liu L, Zheng J, Deng Z, Ma G, Zhang Y and Li J 2007 A two-pole Halbach permanent magnet guideway for high temperature superconducting Maglev vehicle *Physica* C **463–465** 426

[36] Ma G T *et al* 2014 Numerical simulations of the mutual effect among the superconducting constituents in a levitation system with translational symmetry *J. Appl. Phys.* **115** 083908

[37] Ma G-T 2013 Considerations on the finite-element simulation of high-temperature superconductors for Magnetic levitation purposes *IEEE Trans. Appl. Supercond.* **23** 3601609

[38] Ma G-T, Ye C-Q, Liu K, Mei G-M, Zhang H and Li X-T 2016 Geometrical effects on the levitation capability of multiseeded Y–Ba–Cu–O blocks *IEEE Trans. Appl. Supercond.* **26** 3600205

[39] Dias D H N, Sotelo G G, Sass F, Motta E S, de Andrade R Jr and Stephan R M 2012 Dynamical tests in a linear superconducting magnetic bearing *Phys. Proc.* **36** 1049

[40] Sotelo G G, Dias D H, de Andrade R Jr, Stephan R M and Costa G C 2011 Tests on a superconductor linear magnetic bearing of a full-scale MagLev vehicle prototype *IEEE TAS* **21** 1464

[41] Mattos L S, Rodriguez E, Costa F, Sotelo G G, de Anglade R and Stephan R M 2016 MagLev-cobra operational tests *IEEE Trans. Appl. Supercond.* **26** 3600704

[42] Sotelo G G *et al* 2013 Tests with one module of the Brazilian Maglev-Cobra vehicle *IEEE TAS* **23** 3601204

[43] Sotelo G G *et al* 2014 MagLev cobra: test facilities and operational experiments *J. Phys. Conf. Ser.* **507** 032

[44] www.atz-gmbh.com

[45] Werfel F N *et al* 2013 Large-scale HTS bulks for magnetic application *Physica* C **484** 6

[46] Werfel F N *et al* 2011 Recent up-scaling in HTS magnetic device technology *IEEE TAS* **21** 1473

[47] Werfel F N *et al* 2012 Bulk superconductors in mobile application *Phys. Proc.* **36** 948

[48] Werfel F N *et al* 2012 Superconductor bearings, flywheels and Transportation *Supercond. Sci. Technol* **25** 014007

[49] Brown D *et al* 2002 Developments in the processing and properties of NdFeb-type permanent magnets *J. Magn. Magn. Mater.* **248** 432

[50] Sagawa M *et al* 1987 Nd–Fe–B Permanent Magnet Materials *Jpn. J. Appl. Phys.* **26** 785

[51] Ma B M *et al* 2002 Recent development in bonded NdFeB magnets *J. Magn. Magn. Mater.* **239** 418

[52] Halbach K 1985 Applications of permanent magnets in accelerators and electron storage rings *J. Appl. Phys.* **57** 3605

[53] Chang P-Z, Moon F C, Hull J R and Mulcahy T M 1990 Levitation force and magnetic stiffness in bulk high-temperature superconductors *J. Appl. Phys.* **67** 4358

[54] Benu M A *et al* 1987 *Appl. Phys. Lett.* **51** 57

[55] Ramakrishna K *et al* 1988 *Solid Commun.* **65** 831

[56] Benzi P *et al* 2004 *J. Cryst. Growth* **269** 625

[57] Hatano T *et al* 1987 *Jpn. J. Appl. Phys.* **26** L721

[58] Cava R J, Batlogg B, Chen C H, Rietman E A, Zahurak S M and Werder D 1987 *Phys. Rev.* B **36** 5719

[59] Hosoya S *et al* 1987 *Jpn. J. Appl. Phys.,* **26** L325

[60] Kanbe S *et al* 1987 *Jpn. J. Appl. Phys.,* **26** L613

[61] Hikami S *et al* 1987 *Jpn. J. Appl. Phys.* **26** L347

[62] Tamegai T *et al* 1987 *J. Appl, Phys.* **26** L1304

[63] Tarascon J M *et al Phys. Rev.* B **36** 226

[64] Takita K *et al* 1987 *Jpn. Appl. Phys.* **26** L854

[65] Iwata T, Hikita M and Tsurumi S 1989 *Adv. Supercond.* **1** 197

[66] Yoo S I and McCallum R W 1993 *Physica* C **210** 147

[67] Wada T, Suzuki N, Maeda T, Maeda A, Uchida S, Uchinokura K and Tanaka S 1988 *Appl. Phys. Lett.* **52** 1989

[68] Daeumling M, Seuntjens J M and Larbalestier D C 1990 *Nature* **346** 332

[69] Murakami A *et al* 2014 *J. Phys. Conf. Ser.* **507** 012034

[70] Granados X *et al* 1994 *Cryogenics* **34** (suppl. 1) 833

[71] Jin S, Tiefel T H, Sherwood R C, van Dover R B, Davis M E, Kammlott G W and Fastnacht R A 1988 *Phys. Rev.* B **37** 7850

[72] Salama K, Selvamanickam V, Gao L and Sun K 1989 *Appl. Phys. Lett.* **54** 2352

[73] Murakami M, Morita M, Doi K and Miyamoto K 1989 *Jpn. J. Appl. Phys.* **28** 1189

[74] Fujimoto H, Murakami M, Gotoh S, Shiohara Y, Koshizuka N and Tanaka S 1989 *Adv. Superconductivity II* (Tokyo: Springer) 285

[75] Zhou L, Zhang P, Ji P, Wang K, Wang J and Wu X 1990 *Supercond. Sci. Technol.* **3** 490

[76] Shi D, Sengupta S, Luo J S, Varanasi C and McGinn P J 1993 *Physica* C **213** 179

[77] de Rango P, Lees M, Lejay P, Sulpice A, Tournier R, Ingold M, Germi P and Pernet M 1991 *Nature* **349** 770

[78] Morita M, Takebayashi S, Tanaka M, Kimura K, Miyamoto K and Sawano K 1991 *Adv. Supercond.* **3** 733–6

[79] Morita M, Takebayashi S, Tanaka M and Kimura K 1991 *Adv. Supercond.* **3** 733

[80] Yamada Y and Shiohara Y 1993 *Physica* C **217** 182

[81] Walter H 2000 *J. Mater. Res.* **15** 1231

[82] Fuchs G 2000 *Appl. Phys. Lett.* **76** 2107

[83] www.can-superconductors.com

[84] Russell V, Hirst R, Kanda F A and King A J 1953 *Acta Cryst.* **6** 870

[85] Nagamatsu J, Nakagawa N, Muranaka T, Zenitani Y and Akimitsu J 2001 *Nature* **410** 63

[86] Murakami A, Iwamoto A and Noudem J G 2018 *IEEE TAS* **28** 8400204

[87] Safran S, Kılıc A, Asikuzun E, Kılıcarslan E, Ozturk O and Gencer A 2014 *J. Mater. Sci., Mater. Electron.* **25** 2737

[88] Muralidhar M *et al* 2015 *Adv. Eng. Mater.* **17** 831

[89] Muralidhar M *et al* 2015 *Phys. Status Solidi* A **212** 2141

[90] Cardwell D A and Babu N H 2006 *Physica* C **445–448** 1

[91] Iida K *et al* 2005 *Supercond. Sci. Technol.* **18** 1421

[92] Cardwell D A 1998 *Mat. Sc. Engineer.* **B53** 1

[93] Feng Y *et al* 2000 *Supercond. Sci. Technol.* **13** 703

[94] He L-H and Hu G-Q 2001 *Chin. Phys.* **10** 343

[95] Vinod K, Abhilash Kumar R G and Syamaprasad U 2007 *Supercond. Sci. Technol.* **20** R1

[96] Badica P *et al* 2018 *Ceramic Int.* **44** 10181

[97] Tampieri A, Celotti G, Sprio S, Caciuffo R and Rinaldi D 2004 *Phys.* C **400** 97

[98] Noudem J G, Aburras M, Bernstein P, Chaud X, Muralidhar M and Murakami M 2014 *J. Appl. Phys.* **116** 163916

[99] Shim S H *et al* 2005 *J. Am. Ceram. Soc.* **88** 858

[100] Torralba J M 2014 Improvement of mechanical and physical properties in powder metallurgy *Comprehensive Materials Processing* (Elsevier Ltd)

[101] Noudem J G, Dupont L, Gozzelino L and Bernstein P 2016 *Materials Today: Proc.* **3** 545

[102] Sass F, Dias D H N, Sotelo G G and de Andrade Junior R 2018 Superconducting magnetic bearings with bulks and 2G HTS stacks: comparison between simulations using H and A-V formulations with measurements *Supercond. Sci. Technol.* **31** 025006

[103] Dias D H N, Sotelo G G and de Andrade R 2011 Study of the lateral force behavior in a field cooled superconducting linear bearing *IEEE TAS* **21** 1533

[104] Sass F, Sotelo G G, de Andrade R and Sirois J F 2015 H-formulation for simulating levitation forces acting on HTS bulks and stacks of 2G coated conductors *Supercond. Sci. Technol.* **28** 125012

[105] Yang W M, Chao X X, Bian X B, Liu P, Feng Y, Zhang P X and Zhou L 2003 The effect of magnet size on the levitation force and attractive force of single-domainYBCO bulk superconductors *Supercond. Sci. Technol.* **16** 789

[106] Noudem J and Bernstein P unpublished results

[107] Ainslie M D and Fujishiro H 2015 Modelling of bulk superconductor magnetization *Supercond. Sci. Technol.* **28** 053002

[108] Zhou J, Zhang X-Y and Zhou Y-H 2010 Temperature dependence of levitation force and its relaxation in a HTS levitation system *Physica* C **470** 336

[109] Bernstein P, Colson L, Dupont L and Noudem J 2017 Investigation of the levitation force of field cooled YBCO and MgB2 disks as functions of temperature *Supercond. Sci. Technol.* **30** 065007

[110] Sanchez A, Del-Valle N, Navau C and Chen D-X 2009 Critical-current density analysis of force and stability in maglev systems *J. Appl. Phys.* **105** 023906

[111] Qin M J, Li G, Liu H K, Dou S X and Brandt E H 2002 Calculation of the hysteretic force between a superconductor and a magnet *Phys. Rev.* B **66** 024516

[112] Del-Valle N, Sanchez A, Navau C and Chen D-X 2011 Magnet guideways for superconducting maglevs: comparison between halbach-type and conventional arrangements of permanent magnets *J. Low Temp. Phys.* **162** 62

[113] Liao H, Zheng J, Jin L, Huang H, Deng Z, Shi Y, Zhou D and Cardwell D A 2018 Dynamic levitation performance of Gd–Ba–Cu–O and Y–Ba–Cu–O bulk superconductors under a varying external magnetic field *Supercond. Sci. Technol.* **31** 035010

[114] Liu W, Wang J S, Ma G T, Zheng J, Tuo X G, Li L L, Ye C Q, Liao X L and Wang S Y 2012 Influence of lateral displacement on the levitation performance of a magnetized bulk high-Tc superconductor magnet *Physica* C **474** 5

[115] Yang W, Liu Y, Wen Z, Chen X and Duan Y 2008 Hysteresis force loss and damping properties in a practical magnet–superconductor maglev test vehicle *Supercond. Sci. Technol.* **21** 015014

[116] Morandi A 2012 2D electromagnetic modelling of superconductors *Supercond. Sci. Technol.* **25** 104003

[117] Badia A and Freyhardt H C 1998 Meissner state properties of a superconducting disk in a non-uniform magnetic field *J. Appl. Phys.* **83** 2681

[118] Quéval L *et al* 2018 Superconducting magnetic bearings simulation using an H-formulation finite element model *Supercond. Sci. Technol.* **31** 084001

[119] Senatore C, Barth C, Bonura M, Kulich M and Mondonico G 2016 Field and temperature scaling of the critical current density in commercial REBCOcoated conductors *Supercond. Sci. Technol.* **29** 014002

[120] Navau C and Sanchez A 2001 Magnetic properties of finite superconducting cylinders: II. Non uniform applied field and levitation force *Phys. Rev.* B **64** 214507

[121] Sanchez A and Navau C 2001 Magnetic properties of finite superconducting cylinders. I. Uniform applied field *Phys. Rev.* B **64** 214506

[122] Del-Valle N *et al* 2008 A theoretical study of the influence of superconductor and magnet dimensions on the levitation force and stability of maglev systems *Supercond. Sci. Technol.* **21** 125008

[123] Sanchez A, Valle N D, Pardo E, Chen D-X and Navau C 2006 Magnetic levitation of superconducting bars *J. Appl. Phys.* **99** 113904

[124] Prigozhin L 1997 Analysis of critical-state problems in type-II superconductivity *IEEE Trans. Appl. Supercond.* **7** 3866

[125] Prigozhin L 1996 The bean model in superconductivity: variational formulation and numerical solution *J. Comput. Phys.* **129** 190

[126] Bossavit A 1994 Numerical modelling of superconductors in three dimensions: a model and a finite element method *IEEE Trans. Magn.* **30** 3363

[127] Valle N D, Sanchez A, Pardo E, Chen D-X and Navau C 2007 Optimizing levitation force and stability in superconducting levitation with translational symmetry *Appl. Phys. Lett.* **90** 042503

[128] Agramunt-Puig S, Del-Valle N, Navau C and Sanchez A 2013 Optimization of superconducting linear levitation system using a soft ferromagnet *Physica* C **487** 11

[129] Del–Valle N, Sanchez A, Navau C and Chen D-X 2008 Lateral-displacement influence on the levitation force in a superconducting system with translational symmetry *Appl. Phys. Lett.* **92** 042505

[130] Kordyuk A 1998 Magnetic levitation for hard superconductors *J. Appl. Phys.* **83** 610

[131] Hull J R and Cansiz A 1999 Vertical and lateral forces between a permanent magnet and a high-temperature superconductor *J. Appl. Phys.* **86** 6396

[132] Yang Y and Zheng X 2007 Method for solution of the interaction between superconductor and permanent magnet *J. Appl. Phys.* **101** 113922

[133] Wu X-D *et al* 2013 Modeling of hysteretic behavior of the levitation force between superconductor and permanent magnet *Physica* C **486** 17

[134] Zhang M *et al* 2017 The connection characteristics of flux pinned docking interface *J. Appl. Phys.* **121** 113907

[135] Yang W *et al* 2018 Effects of magnetization conditions on dynamic characteristics of spacecrafts with superconducting flux pinning docking interfaces *J. Appl. Phys.* **124** 213901

[136] Bernstein P, Noudem J and Dupont L 2016 Critical current density and current distribution in field cooled superconducting disks *Supercond. Sci. Technol.* **29** 075007

[137] Brandt E H 1998 Superconductor disks and cylinders in an axial magnetic field. I. Flux penetration and magnetization curves *Phys. Rev.* B **58** 6506

[138] Bernstein P *et al* 2018 A new approach to the current distribution in field cooled superconductors disks *Supercond. Sci. Technol.* **31** 015008

[139] Chen I-G, Liu J, Weinstein R and Lau K 1992 Characterization of YBa$_2$Cu$_3$O$_7$ including critical current density J$_c$ by trapped magnetic field *J. Appl. Phys.* **72** 1013

[140] Huang C-G *et al* 2019 *Supercond. Sci. Technol.* **32** 045002

[141] Floegel-Delor U *et al* 2019 *IEEE Trans. Appl. Supercond.* **29** 3601705

[142] Sun R X *et al* 2017 Design and fabrication of a hybrid maglev model employing PML and SML *Int. J. Mod. Phys.* B **31** 1745014

[143] Martins F G R *et al* 2018 *IEEE Trans. Appl. Supercond.* **28** 6602405

[144] Sass F *et al* 2012 Coated conductors for the magnetic bearing application *Phys. Proc.* **36** 1008

[145] Liu K *et al* 2018 Experiment and simulation of superconducting magnetic levitation with REBCO coated conductor stacks *Supercond. Sci. Technol.* **31** 015013